The Thesis Committee for Abigail A. Tomasek
Certifies that this is the approved version of the following thesis:

Hydrodynamic Flow Modeling of Barton Springs Pool

APPROVED BY
SUPERVISING COMMITTEE:

Supervisor:

Ben R. Hodges

Paola Passalacqua

Hydrodynamic Flow Modeling of Barton Springs Pool

by

Abigail A. Tomasek, B.C.E; B.S.

Thesis

Presented to the Faculty of the Graduate School of

The University of Texas at Austin

in Partial Fulfillment

of the Requirements

for the Degree of

Master of Science in Engineering

The University of Texas at Austin

August 2013

Acknowledgements

I would like to thank my advisor, Ben Hodges, for his guidance and mentorship over the past two years. I would like to thank the City of Austin for providing funding for the project, and, in particular, Liza Colucci and Laurie Dries who provided support in late night data collection and an endless supply of information on Barton Springs Pool. I would also like to acknowledge the entire staff at Barton Springs Pool in their patience and adaptability for the project's data collection requirements. Thank you to my second reader, Paola Passalacqua, for the helpful feedback on my thesis. To my friends and family, thank you for providing support and guidance throughout my thesis work, particularly David Christiansen for your help in Matlab scripting, data collection, project construction, and moral support. Justin Camp provided essential discharge data and the University of Texas Bureau of Economic Geology provided lidar data and high-quality imaging of the Barton Springs Pool area.

Abstract

Hydrodynamic Flow Modeling of Barton Springs Pool

Abigail A. Tomasek, M.S.E.

The University of Texas at Austin, 2013

Supervisor: Ben R. Hodges

Barton Springs Pool (BSP) is an important ecological and recreational resource to the City of Austin (CoA). Due to sediment accumulation, excessive algal growth, and concern for water velocities through salamander habitat, improving the flow regime of BSP was identified as an important focus for future infrastructure development in Barton Springs Pool. The CoA commissioned this project to develop and test a hydrodynamic model to provide a basis for understanding the flow dynamics of BSP, and to aid in future infrastructure developments in BSP. This phase of the project included the collection of bathymetric and velocity data, creating a hydrodynamic model of BSP that dynamically represents space-time varying 3D velocities, and testing the model using the default settings and an adjustment of the outlet coefficients. The model was run with three targeted inflow scenarios to determine both how the model responds with varying inflows, and to provide a general idea of how flow in BSP is affected by the magnitude of the inflow.

The model used was the Fine Resolution Environmental Hydrodynamic Model that solves the 3D non-hydrostatic Navier-Stokes equations in a split hydrostatic/non-hydrostatic approach. The model was run using the default settings and the outputs were compared to available data. Results from these initial runs showed that further calibration is necessary. Model runs under the targeted inflow scenarios showed that as inflow increases, velocities in the upstream portion of BSP increase correspondingly, but this is not reflected in the downstream portion of BSP.

Table of Contents

List of Tables

List of Figures

Chapter 1. Introduction

1.1 Overview

The following report describes the hydrodynamic flow modeling of Barton Springs Pool (BSP) and includes discussion on the field data collection, modeling, and initial results from the BSP hydrodynamic model. The collected field data include bathymetric data acquired using sonar equipment, velocity data collected using two Acoustic Doppler Current Profiler (ADCP) instruments, and discharge data. The model used for the project was the Fine Resolution Environmental Hydrodynamic Model (FREHD) version PC2v7g, developed at the Center for Research in Water Resources (CRWR), University of Texas at Austin. The uncalibrated model was run under default conditions and the calibrated model will be used in the future for testing different arrangements of inlet and outlet structures at different flows to evaluate infrastructure issues in BSP.

1.2 Site Description

BSP is an important ecological and recreational resource to the City of Austin. Its near constant 70˚F provides relief during the hot Austin summers and for dedicated lap swimmers year round. The Barton Springs Salamander, *Eurycea sosorum*, was listed as a federally endangered species in May 1997 (U.S. Fish and Wildife Service, 1997), and is known to only inhabit the springs in Zilker Park in the City of Austin, collectively called the Barton Springs Complex (Chippindale, Price, and Hillis, 1993).

The Barton Springs system consists of four natural springs, Main Barton Spring (also known as Parthenia Spring), Eliza Spring, Old Mill Spring (also known as Sunken Garden or Zenobia Spring), and Upper Barton Spring. These springs are all fed through groundwater discharging from the Barton Springs segment of the Edwards Aquifer, which is hydrologically distinct from the rest of the Edwards Aquifer. The Barton Springs segment is approximately 155 square miles and represents about 4% of the total area of the Edwards Aquifer; about 151 square miles of the Barton Springs segment discharge to Barton Springs, and the remaining 4 square miles discharge to Cold and Deep Eddy Springs (Slade, Dorsey, and Stewart, 1986). It is estimated that 85% of the Barton Springs segment of the Edward Aquifer's recharge occurs on the main channels of six creeks that cross the recharge zone (Slade et al., 1986). These creeks' watersheds are divided into the contributing, recharge, and confined zone. Water flows over the contributing zone and into the recharge zone, where the outcrop of the Edwards limestone is at the land surface, allowing for water to freely flow into the karstic limestone pores and channels. Once in the aquifer, groundwater generally follows the northeastward strike of the Balcones fault zone toward Barton Springs, the lowest point of hydraulic pressure (Slade et al., 1986). Discharge from the Barton Springs system reflects aquifer conditions, where high water-levels in the aquifer cause high spring discharge (Mahler, Musgrove, Sample, and Wong, 2011), and under low aquifer water levels, discharge from Main Barton Springs decreases and discharge ceases from the smaller springs.

Of the four natural springs that make up the Barton Springs system, the largest is Main Barton Spring, which emerges from fissures just west of the diving board in BSP.

The discharge from Main Barton Springs can be categorized as low flow (less than 40 cfs, 1.13 m^3/s), average flow (40 to 89 cfs, 1.13 to 2.52 m^3/s), and high flow (greater than 90 cfs, 2.55 m^3/s) (Mahler, Garner, Musgrove, Guilfoyle, and Rao, 2006). Discharge from the Barton Springs complex has ranged from 10 to 120 cfs (0.28 to 3.40 m^3/s), with a long-term average flow of 53 cfs (1.5 m^3/s) (Scanlon et al., 2001).

1.3 Existing BSP Infrastructure

Two dams were built in the late 1920s, forming a natural swimming pool with nearly two acres of water surface (Limbacher and Godfrey, 2008). Historically, the upstream dam had three openings allowing streamflow from Barton Creek to flow through BSP (Tuchsherer, Schroeder, and King, 2011). However, these openings were closed in 1975 as part of the bypass tunnel construction. The bypass tunnel diverts Barton Creek flow around BSP through a concrete culvert under the walkway on the north side of BSP, where it also captures flow from Eliza Spring that had historically flowed into BSP. The water diverted by the bypass joins with water discharging from the downstream BSP dam and continues as Barton Creek. Through the construction of the bypass, the only inflow to BSP under normal-flow conditions is from springflow from Main Barton Springs, except when occasional floodwaters from Barton Creek overtop the upstream dam.

The downstream dam's outlet structures consist of four 2 x 2 ft (0.6 x 0.6 m) gates, two spillways with 3 ft (0.9 m) widths, three spillways with 5 ft (1.5 m) widths, and a 3.5 in. (0.09 m) diameter pipe. Additional outflows occur through a 2 ft (0.61 m) diameter

pipe in the bottom substrate of the pool near the upstream dam that runs along the length of the pool, discharging into the bypass culvert on the north side of BSP near the diving board[1]. The gates are opened for drawdowns of the pool, which is allowed only four times a year with the additional requirement that the Barton Springs' complex discharge is above 54 cfs (1.54 m^3/s) (City of Austin, 1998) during openings. Drawdowns are performed to allow for easier and more thorough cleaning of BSP. During droughts, the three center spillways are closed to keep BSP water levels consistent with the depths indicated along the pool sidewalks. The elevation of the water surface is maintained at an almost constant elevation of 433 ft (132 m) above mean sea level (MSL), with variations of 1-2 in. due to different environmental conditions[2].

When this project commenced in September 2011, water from BSP was leaking into the bypass culvert due to the deterioration of the bypass. Construction to repair the culvert began in October 2012 and ended in April 2013.

1.4 Motivation

This project was undertaken due to several problems occurring in BSP, including sediment accumulation, excessive algal growth, and concern for water velocities through salamander habitat that could be impacted by the infrastructure of BSP. From a hydraulic standpoint, BSP presently acts as a slow-moving pond with salamander habitat affected by the availability of moderate velocity conditions, and appropriate substrate (Limbacher

[1] Dimensions and locations for the outlets were determined using plans provided by the CoA and by direct measurements of the outlets by the CRWR research team.
[2] L Dries, City of Austin, pers. comm. 2012.

and Godfrey, 2008). Slow-moving waters also encourage algae growth, which leads to slippery pool surfaces and unaesthetic floating materials. These problems are exacerbated during drought conditions when flows are at their lowest. Because of these reasons, improving the flow regime was identified as an important focus for future infrastructure development in BSP. To provide a basis for understanding the flow hydrodynamics in BSP, a hydrodynamic model was commissioned by the CoA. Phase I of this project, the focus of this report, represents the development and testing of this model.

1.5 The Hydrodynamic Model

1.5.1 Introduction

Hydrodynamic models provide an effective way to visualize water flow and have been used to investigate a range of hydrologic processes and phenomena, such as internal waves (Wadzuk and Hodges, 2004), hurricane storm surges (Westerink et al., 2008), and eutrophication (Cerco and Cole, 1993). For this project, the CoA commissioned the creation of a hydrodynamic model to understand the flow dynamics of BSP and the model will be used to see how different arrangements of inlet and outlet structures affect flow through BSP. While studies have investigated water flow through the Barton Springs portion of the Edwards Aquifer (Slade et al, 1986; Hunt, Banda, and Smith, 2010), this is the first modeling effort for flow through BSP.

1.5.2 The BSP Hydrodynamic Model

Three-dimensional (3D) hydrodynamic models for lakes, estuaries, and rivers generally use the hydrostatic approximation, which neglects non-hydrostatic pressure and vertical acceleration (Wadzuk and Hodges, 2004). Based on past use and validation, the hydrostatic approximation is reasonable for large-scale predominately horizontal phenomena (Hodges, Laval, and Wadzuk, 2006; Kantha and Clayson, 2000). The BSP model was initially run using the hydrostatic approximation, but the numerical modeling experiments during this project indicated that vertical accelerations could not be neglected near the spring inflow or the spillways in the downstream dam, so a non-hydrostatic component was added to the model to capture the effects of vertical acceleration and non-hydrostatic pressure gradients. Previous studies also found that rapidly changing bathymetry, which is present in BSP, can cause hydrostatic assumptions to fail (Koçyigit and Falconer, 2004; Wadzuk and Hodges, 2004; Weilbeer and Jankowski, 2000).

BSP was modeled using a 3D hydrodynamic model of time-evolving flow, specifically using the FREHD model. The FREDH model solves the 3D non-hydrostatic Navier-Stokes equations in a split hydrostatic/non-hydrostatic approach. The hydrostatic solution is considered a first approximation of the flow, which is solved using a semi-implicit method based on the TRIM model (Casulli and Cheng, 1992; Casulli and Cattani, 1994). The non-hydrostatic solution is solved as a small correction to the hydrostatic soluction (Casulli and Zanolli, 2002). FREHD is built on ideas originally developed in the Estuary and Lake Computer Model (ELCOM) writted by Hodges and

others (Hodges et al., 2000; Wadzuk and Hodges, 2009; Dallimore et al., 2003; Botelho et al., 2009) that has been applied to at least 24 lakes around the world (Hodges, 2013). The description of the governing equations and discretization methods for FREHD are found in Hodges and Rueda (2008) and Wadzuk and Hodges (2009).

1.6 Objectives

The objectives of this project were to:

1. Collect data required for the development and calibration of the hydrodynamic model of BSP, including bathymetric, velocity, and discharge data.
2. Create a hydrodynamic model (FREHD version PC2v7g) of BSP that dynamically represents space-time varying 3D velocities, specifically under three base flow scenarios (≤30 cfs, 40-70 cfs, and ≥85 cfs).
3. Run the model using default settings and compare modeled discharges to measured discharges, perform a drag coefficient sensitivity analysis, and compare modeled velocity data to collected ADCP velocities.

1.7 Organization of this Report

This report discusses the use of the FREHD model for the hydrodynamic modeling of BSP. Section 3 provides an overview of the data collection methods and analysis to meet Objective 1. Detailed explanations of the collection methods and processing of collected data are provided in Appendix A, B, and C. Section 3 discusses the methodology and inputs of the FREHD model, while §4 discusses the model runs and testing to meet Objectives 2 and 3.

Chapter 2. Data Collection and Analysis

2.1 Overview

Two types of data were required for this project: bathymetry (depth) data describing the bottom topography of BSP, and velocity data providing the magnitude and direction of flow. Bathymetry data was collected over four days and statistically processed to produce a 0.86 x 0.86 m (2.8 x 2.8 ft) gridded bathymetry. Velocity data was collected using two approaches: (1) a mobile Acoustic Doppler Current Profiler (ADCP) that provided a near-synoptic measurement of the velocity field over most of BSP for a single survey time interval, and (2) a fixed ADCP that provided velocity profiles at fixed locations over time.

2.2 Bathymetric Data Collection

Since BSP is a natural system with spatially varying bathymetry, a fine-scale elevation map is required for hydrodynamic modeling. A customized bathymetric survey unit was constructed for this project. The survey unit was positioned in BSP with two nylon lines controlled by two people on either side of the pool. Single transects of depth data with corresponding GPS positions were acquired by slowly pulling the survey unit across BSP. Approximately 620 transects were collected in 1.5 ft (0.46 m) increments along the length of BSP. These depth data were used to create the bathymetric map for the hydrodynamic model.

The bathymetric survey unit consisted of a Lowrance® HDS-5 Fish Finding Sonar and GPS unit and a Lowrance® LSS-2 StructureScan™ Sonar Imaging unit, both of which are designed for fishing applications but provide a low-cost approach to collecting depth and position data. The HDS unit has a built-in GPS antenna and comes equipped with Wide Area Augmentation System (WAAS) for improved positional accuracy (§2.3). The transducers for both units send sonar waves into the water and determine depth by the travel time of the echoes. The HDS unit has an SD memory card slot and a SanDisk 8GB Ultra SDHC memory card was used to continuously collect bathymetric data from both units.

The framework for the bathymetry survey unit was a waterproof 5 gallon bucket floated by a 3 ft diameter inflatable child's swimming tube with a fabric bottom. The HDS sonar/GPS was mounted to the lid of the bucket so that the control could be accessed without breaking the watertight bucket seal. The StructureScan control system was placed inside the bucket along with a 12V battery for power (Figure 2.1). The bucket was placed in the inflatable tube, and the gaps between the tube and the bucket were filled with pieces of closed-cell foam to aid in flotation and to prevent the bucket from shifting. The transducers for both sonar units were mounted on a piece of plywood that had been coated in epoxy resin for strength, and the plywood was attached to the bottom of the inflatable tube. The StructureScan transducer was mounted 6 inches from the HDS transducer so that depths recorded by both instruments could be correlated. When deployed, the transducers were approximately 4 inches below the water surface. To maintain watertight integrity, holes that were cut in the bucket for cables were sealed

with gaskets, epoxy, and 3M 5200 Marine Sealant. The 8 amp-hour 12V battery used to power the units typically lasted about four hours before requiring replacement with a fresh battery. Appendix A.1 discusses the wiring and powering of the bathymetric survey unit.

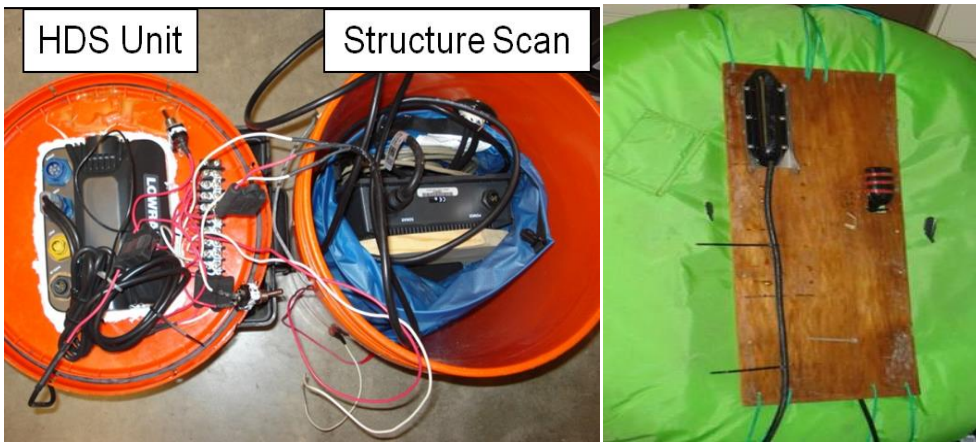

Figure 2.1. Bathymetric equipment setup (A) Lowrance HDS and StructureScan units as installed (B) The two transducers mounted to plywood and attached to the bottom of the inflatable tube.

Bathymetric data were collected on four survey dates, shown in Table 2.1. The HDS settings used for the survey unit are listed in Table 2.2; manufacturers default settings were used for the StructureScan. BSP's operational policy required all surveying to be completed within 2000 to 0500 hours when the pool was closed to the public. Although a pulley system was designed and initially used for pulling the survey unit across the pool, it was found that it was simpler to have the lines connected to either side of the inflatable tube and hand-controlled by two persons, one on the north and one on the south side of BSP (Figure 2.2). In the upstream sections of the pool, the natural shoreline made it necessary for one person to be physically in the water. In water depths

of less than 2 ft (0.6 m), the sonar output was noisy, providing unrealistic depths that required correction (see §2.4).

Table 2.1. Bathymetric survey information. All transects are approximately 1.5 ft intervals.

Date	Time commenced	Time completed	Number of transects	Notes
4/15/2012	2224	0415	176	Transects from 0 to 264 ft upstream of downstream dam
4/16/2012	2315	0130	0	GPS errors; unable to obtain valid satellite locations.
4/23/2012	2259	0430	125	Transects from 265.5 to 453 ft upstream of downstream dam
4/29/2012	2200	0430	131	Transects from 454.5 to 651 ft upstream of downstream dam
4/30/2013	2158	0415	188	Transects from 652.5 to 934.5 ft upstream of downstream dam

Table 2.2. HDS sonar settings (other than defaults), see Lowrance (2011a) for further detail.

Setting	Used	Notes
Depth:	shallow < 100 ft	Maximum depth recorded in BSP was 4.8 m (15.75 ft)
Sensitivity	74 to 78	Increasing sensitivity increases clutter on screen display.
Noise rejection	low	Not needed as noise is typically from boat mechanical/electrical sources.
Surface clarity	off	Not needed as clarity is typically affected by surface effects not present in BSP.
Transducer type	Generic 83/200kHz	Select the transducer model connected to the display unit. Incorrect setting causes errors in depth data.

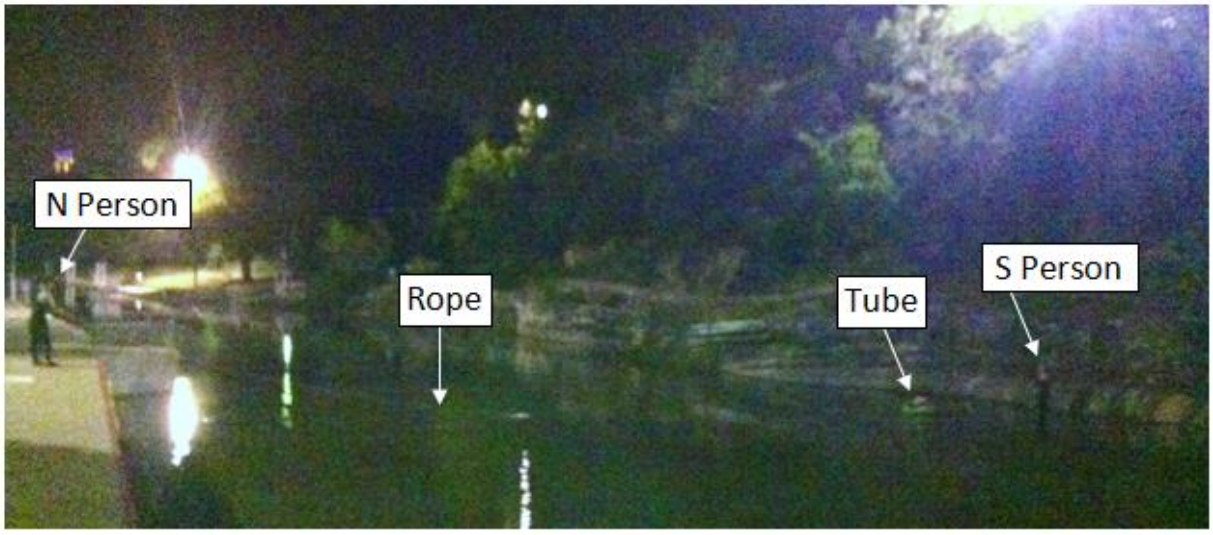

Figure 2.2. Data collection setup for the upstream portion of BSP on April 30, 2012.

2.3 Survey Accuracy

The conventional GPS system provides a worst-case positional accuracy of 7.8 m (25.6 ft) (GPS.gov, 2013), which is not sufficient for a bathymetric survey of BSP. However, the Wide Area Augmentation System (WAAS) for the USA provides nominal horizontal accuracy of 1.6 m (5.25 ft) (FAA, 2008) and is known to achieve accuracies on the order of 0.6 m (1.97 ft). The Lowrance HDS GPS unit is WAAS capable, but had difficulty retaining WAAS reception during the BSP survey. A number of transects had to be repeated after resetting the HDS receiver and re-entering the setup of Table 2.2. It is hypothesized that this problem was caused by the location of the WAAS satellites over the equator and the steep slopes to the south of BSP. Unfortunately, the logging system for the Lowrance unit does not include data entries for WAAS and non-WAAS positions. Statistical processing of the data (§2.4) was used to remove data outliers that were thought to be erroneous.

2.4 Processing the Position-Depth Data

The collected bathymetric data consists of more than 4 million individual depths recorded during the transects outlined in Table 2.1. The data recorded by the Lowrance HDS system has 1 m precision providing 10,740 unique positions within the boundaries of BSP. Thus, on the order of 740 depth measurements are available for each 1 m^2 area of the pool, which form a 0.86 x 0.86 m raster of grid cells. The data for each cell is statistically processed to remove outliers and to generate the bathymetric map of the pool.

The data recorded on the SD card for the HDS and StructureScan units is stored in a *sl2* file format, which is a custom format of the Lowrance Corporation. This file format can be viewed in the Lowrance Sonar Log Viewer, a downloadable PC-based software application that plays back recorded files (Lowrance 2011b). The Sonar Viewer provides three views of the data along any transect: HDS, downscan, and sidescan. The StructureScan images were clear enough to show what the bottom surface and macrophytes looked like in an area.

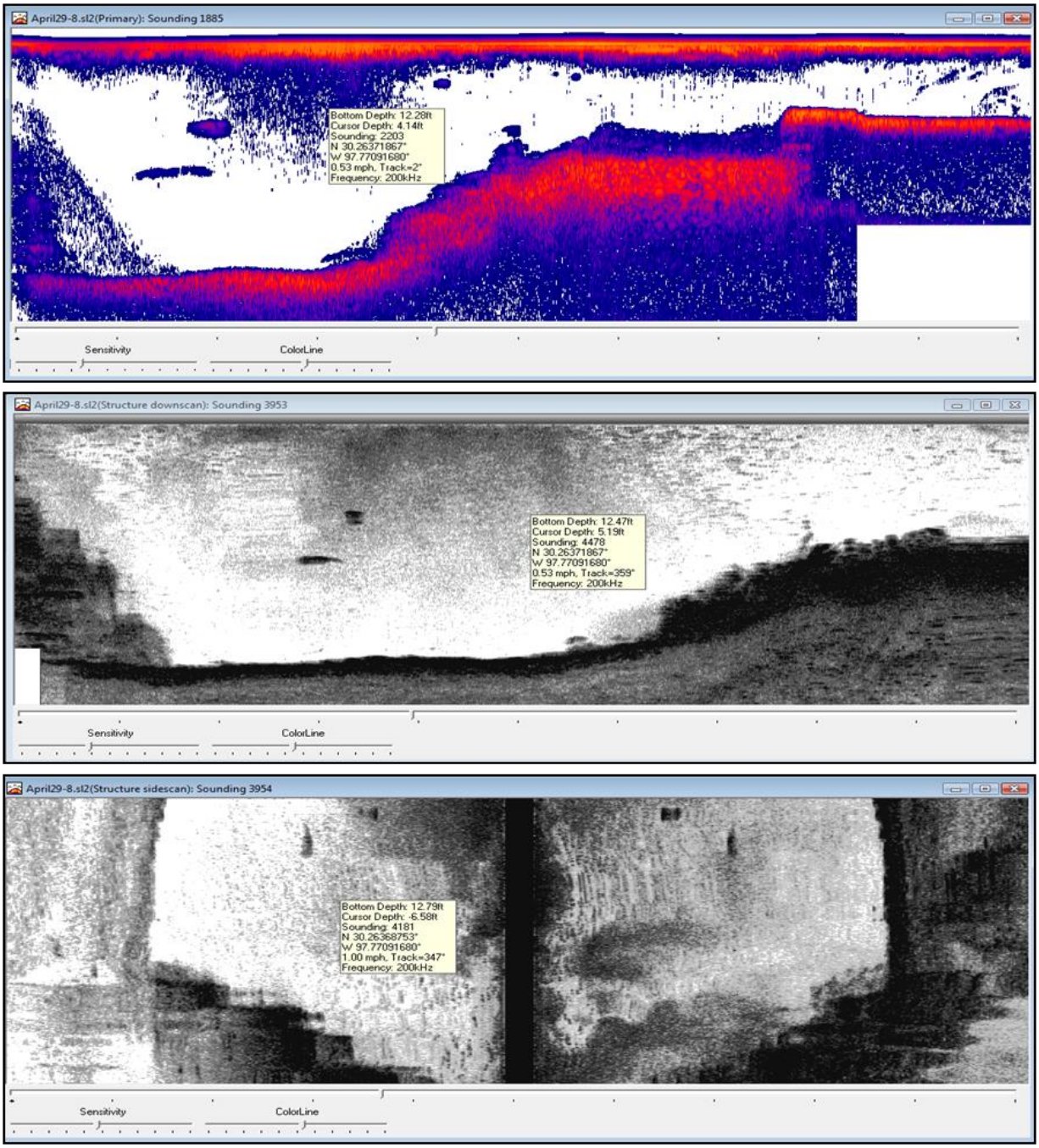

Figure 2.3. Images from Lowrance's Sonar Viewer software showing bottom surface, macrophytes, and fish, (A) from the HDS unit, (B) from the StructureScan downscan, and (C) from the StructureScan sidescan

The bathymetric data from both the StructureScan and conventional HDS transducer were combined into a single data set for analysis. Because the GPS precision produced multiple data at a single point, the bathymetry processing focused on removing outliers and using mean values to create the bathymetric map. Bathymetric processing was conducted in six steps:

1. Removal of depths beyond minimum (0.08 m) and maximum (6 m) values.
2. Compute the mean (μ) and standard deviation (σ) for each 0.866 x 0.866 m cell.
3. Remove depths outside of $\mu \pm \sigma/2$ or $\mu \pm 1$ m for each cell and compute new mean values.
4. Smooth the depth by averaging the mean depth of each cell with its 8 grid neighbors.
5. Identify cells outside of the physical boundary of BSP and remove this data.
6. Identify cells with no data and interpolate data from neighboring cells.

The above process screens out depth data that were erroneously located at a position due to errors in the GPS. Results after Steps 2, 3, and 6 are shown in Figure 2.4 (A, B, and C, respectively). Note that Steps 1 through 4 include position-depth data for positions outside of BSP due to both errors in the GPS position (§2.3) and data collected while the survey system was outside of the pool. These data were removed in Step 5 by using the pool boundary identified from satellite photographs in Google Earth (§D.1). Small areas of BSP were missing data, either due to high velocities near the spillways, non-straight transects, or GPS issues, which were corrected for in Step 6. Figure 2.4(C) shows the final processed bathymetric map that was used as an input in the FREHD model. Appendix A.2 discusses the processing of the position-depth data in more detail.

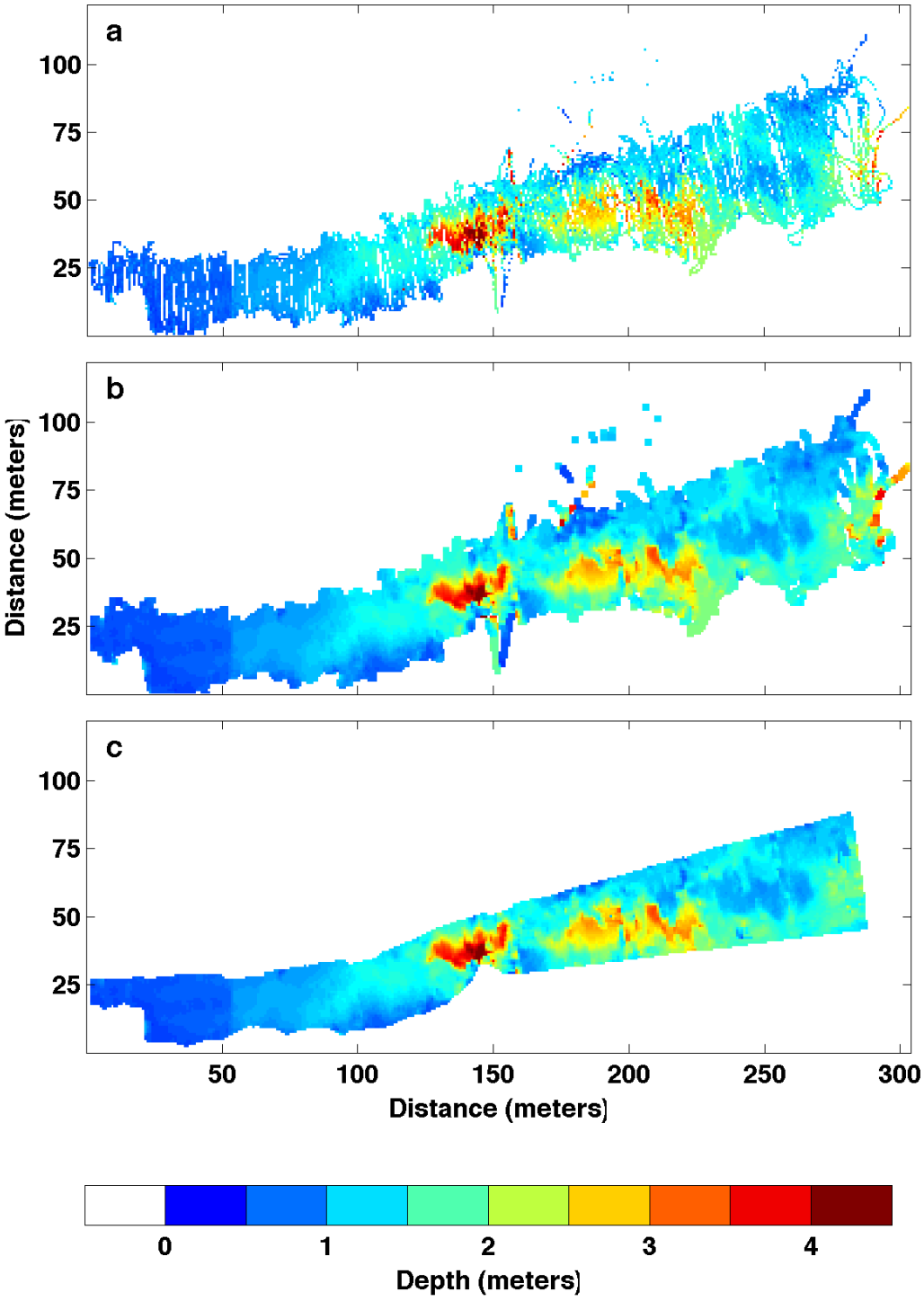

Figure 2.4. Mean depths in meters for offset location through data processing after steps 2 (A), 4 (B), and 6 (C).

As a check on the repeatability of the survey, Quality Assurance (QA) transects were conducted at four locations, approximately 65, 125, 340, and 610 ft upstream from the downstream dam as listed in Table 2.3 and detailed in §A.3. The QA data was processed separately following the same steps as the other bathymetric data. The percent difference was calculated between each QA location on each night and the bathymetry used as a model input. Table 2.4 shows the average and maximum percent difference for each QA transect on each night.

Table 2.3. Date and time of QA transects were collected. Note n/a means that particular QA transect was not collected on that night.

Date	QA1 Time	QA2 Time	QA3 Time	QA4 Time
4/15/2012	2342	0050	n/a	n/a
4/23/2012	0239	0246	2317	n/a
4/29/2012	2200	2229	2244	0258
4/30/2012	2158	2207	2216	2233

Table 2.4. Average and maximum percent differences (PD) between each QA transect on each night and the model input bathymetry (Figure 2.4 C).

Date	Average PD QA1	Max PD QA1	Average PD QA2	Max PD QA2	Average PD QA3	Max PD QA3	Average PD QA4	Max PD QA4
4/15/2012	4.46	16.1	3.29	33.3	n/a	n/a	n/a	n/a
4/23/2012	3.44	10.8	3.91	17.3	8.69	46.4	n/a	n/a
4/29/2012	5.48	18.7	4.24	31.9	16.1	73.4	1.49	5.74
4/30/2012	4.53	25.7	2.99	11.1	11.1	69.7	1.85	9.39

2.5 Synoptic Velocity Data

Synoptic velocity data provides a multi-dimensional representation of the velocity field throughout BSP over a relatively short time interval. The data collection was accomplished with a mobile ADCP instrument mounted on a kayak. Two deployments were conducted (Table 2.5): the first was a partial survey to test the equipment and was

done before the bypass repairs (§1.3); the second deployment was a complete survey of BSP conducted after the bypass repairs.

Synoptic velocity data was collected with a SonTek/YSI M9 ADCP, which is a mobile, downward-looking instrument that measures a velocity profile through the water column using the Doppler shift of high frequency sound waves that reflect from particles in the water. The M9 system also collects bathymetry, GPS position and has a bottom-tracking algorithm used for positioning. The M9 has a profiling range of 0.2 to 40 m (0.66 to 131 ft). Velocity profiles are collected in discrete vertical "cells" (the equivalent of statistical bins) that adjusts to each profile, with the cell size and number of cells changing depending on the M9 velocity measurement resolution at that point (Appendix B.2). Figure 2.5 shows the features of the instrument, which includes two sets of velocity and depth measurement transducers (four 3.0-MHz transducers and four 1.0-MHz transducers), and one 0.5-MHz vertical acoustic beam (echo sounder) that provides depth data only. A power and communications module (PCM) connects the ADCP to a rechargeable battery pack. The M9 communicates data to a PC using a wireless Bluetooth linkage. The GPS positioning for the M9 uses the SonTek Differential GPS (DGPS) system that provides sub-meter accuracy (SonTek 2012a). Data collection, viewing, and processing for the M9 is accomplished with the RiverSurveyor™ and HydroSurveyor™ software. The former was designed for cross-section velocity/discharge surveys of rivers, but was the only software available at the time of the first deployment. The latter software is more appropriate for the BSP survey, and was available for the second deployment.

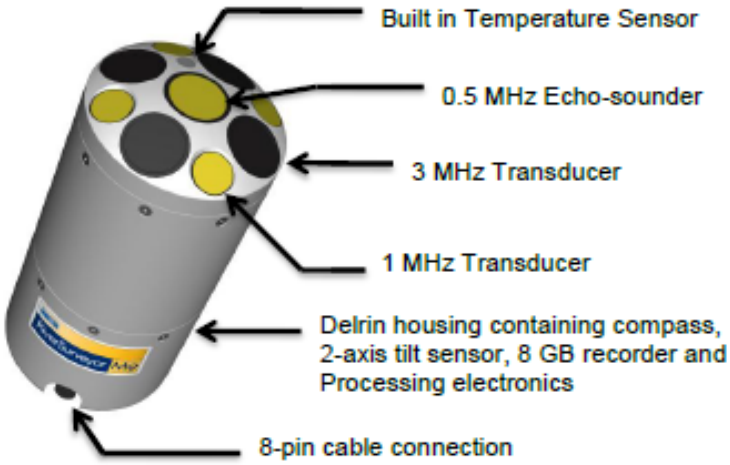

Figure 2.5. The SonTek M9 ADCP instrument (SonTek 2012a).

The M9 was mounted in a sit-on-top kayak (Ocean Kayak Corporation, model Venus 11) for data collection in BSP. A hole was cut through the boat so that the ADCP could be mounted directly on the centerline, as shown in Figure 2.6. Wood blocks were used to provide structural rigidity around the hole, which was sealed by a metal air duct vent, epoxy resin, and 3M 5200 Marine Adhesive sealant. The other electronics for the ADCP were mounted in a waterproof Pelican^{TM} case and connected by cabling through a hole sealed with 3M 5200. Appendix B.1 provides further detail on the collection of synoptic velocity data.

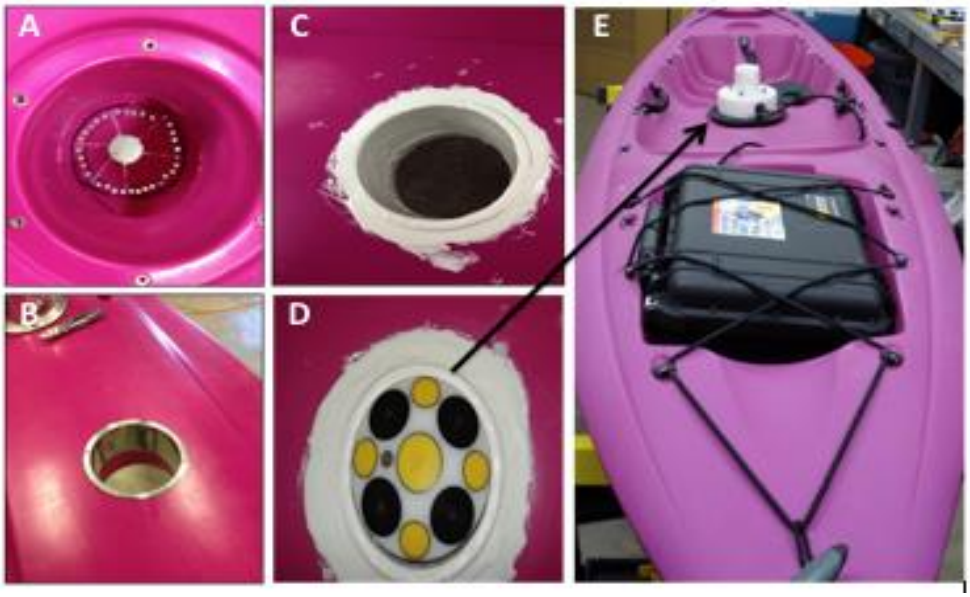

Figure 2.6. ADCP mounting in kayak: (A) hole cut in boat, (B) hole sealed with a metal air duct vent, (C) 3M 5200 Marine Adhesive sealant applied around the vent, (D) ADCP resting in hole, (E) final M9 ADCP setup.

Deployment 1 (Table 2.5) included some data collection in the deeper downstream section of BSP, but was primarily focused on areas near the outlet of Main Barton Springs to the west of the diving board as shown in Figure 2.7. Although the M9 was used with the SonTek DGPS system that is supposed to provide sub-meter positioning accuracy, it can be seen in Figure 2.7 that some of the reported positions are outside the physical boundaries of BSP, despite the fact that the boat was not removed during the survey. These errors appear to be similar to those discussed in §2.3. The complete ADCP data set comprises flow speed and velocity over depth at 5,153 profiles.

Table 2.5. Mobile ADCP Deployments.

Deployment	Date	Software	Time started	Time ended	Number of profiles	Total distance (m)	Average Cell Size (m)	Purpose
1	August 2, 2012	River Surveyor	2235	0200	5153	1430	0.046	Survey of velocities in BSP, focusing on the inflow area of Main Barton Spring near the diving board
2	May 6, 2013	Hydro Surveyor	2250	0245	11379	9000	0.054	Collection of ADCP profiles for all possible areas of BSP.

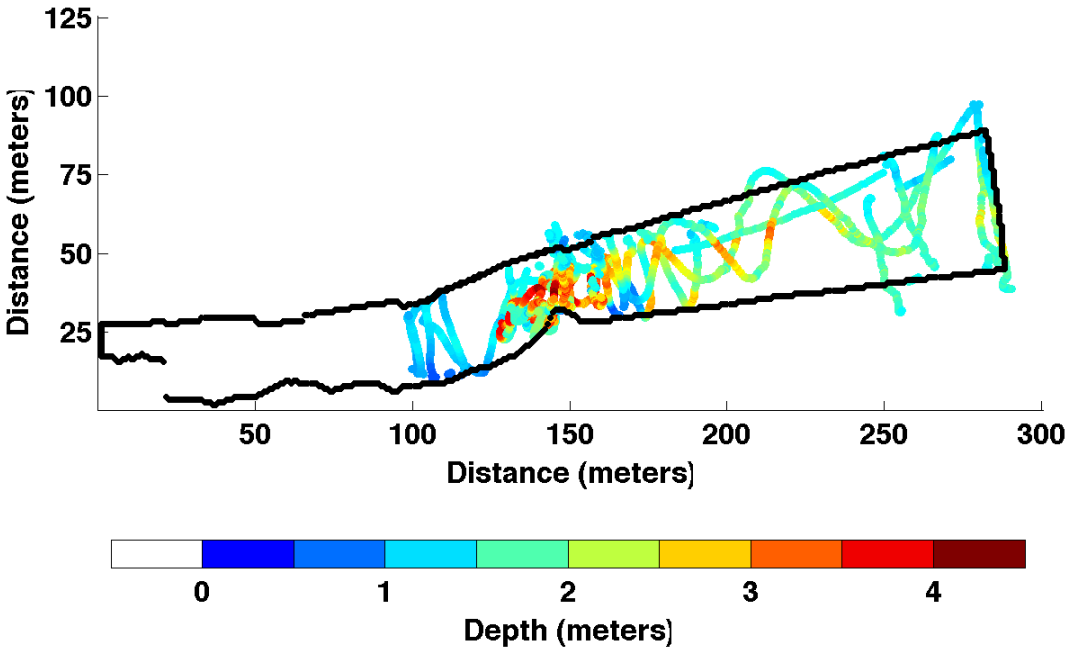

Figure 2.7. Positions and depths for ADCP data collected during the August 2, 2012 survey using RiverSurveyor.

Deployment 2 (Table 2.5) was conducted after the completion of bypass repairs by the CoA in April 2013. This survey covered all of the BSP that was accessible to the boat (depths > 0.5 m, 1.6 ft). Data was collected in parallel transects along the length of

BSP, perpendicular to the main direction of flow, as suggested in Fong and Monismith (2004) for weak currents. Figure 2.8 shows all of the data points along with the water depth in m at that point as measured by the SonTek M9. At each of these locations, at least one velocity profile was collected.

The velocity data from both deployments were processed using the SonTek software, and exported to Matlab for analysis and comparison to model data. Details of the data processing are provided in Appendix B.2.

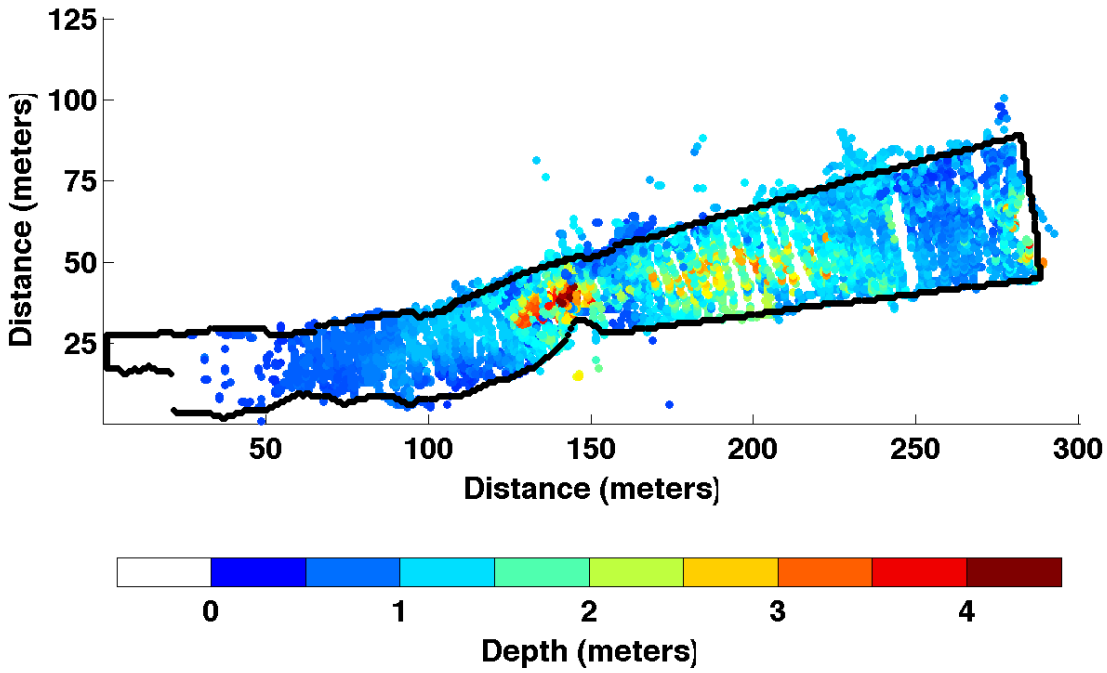

Figure 2.8. Positions and depths of ADCP data collected during the May 6, 2013 survey using HydroSurveyor.

2.6 Temporally-Evolving Velocity Data

A fixed-position, upward looking ADCP was deployed in four different locations (Table 2.6). This approach provides data at limited locations compared to the synoptic data collection, but provides insight over longer time scales than is possible with synoptic measurements. The fixed-position data was collected with a SonTek Argonaut ADCP unit, which consists of two pieces: the ADCP instrument itself, and a battery pack (Figure 2.9). The Argonaut collects velocities in two formats: MultiCell, where velocities for user-specified cells in a profile with a specified blanking distance and maximum depth (Table 2.7) are recorded, and as a dynamic velocity, where a single depth-averaged velocity is recorded.

The deployment locations were in a deep portion of BSP north of the diving board (deployed the same night as the synoptic velocity data collection) and downstream of the spring outflows near Main, Little, and Side Spring[3]. Figure 2.10 shows the deployment locations along with known locations of springs, fissures, and concrete pipe. The ADCP was deployed with the configuration parameters listed in Table 2.7. During Deployment 2, the instrument appeared to have been moved during the first day by recreational swimmers, after which the instrument mounting plate was attached to concrete blocks with rope, deterring any further disturbance. More information on the collection and processing of the fixed-position ADCP data is described in Appendix B.3 and B.4.

[3] As discussed with L. Dries, CoA

Table 2.6. The four deployment locations for the SonTek Argonaut. Model cell is the (row, column) location in the raster grid of the hydrodynamic model (see §D.3). Deployment duration was measured from when the Argonaut was placed in position until when it was moved from the initial location (either due to the public interfering with the Argonaut or at the end of data collection).

Location	Description	Time begin	Time end	Latitude	Longitude	Model Cell	Depth min, m (ft)	Depth max, m (ft)	Number of profiles
1	North of diving board	May 6, 2013 22:37	May 6, 2013 22:58	30.26383	97.77067	(186, 54)	2.9 (9.6)	2.9 (9.6)	128
2	Main Spring	May 30, 2013 10:45	May 30, 2013 21:45	30.26371	97.77086	(165, 40)	4.6 (14.9)	4.6 (15.2)	3,936
3	Little Main	June 3, 2013 11:00	June 5, 2013 10:10	30.26374	97.77089	(162, 43)	3.6 (11.7)	3.7 (12.0)	16,979
4	Side Spring	June 5, 2013 11:00	June 7, 2013 10:20	30.26372	97.77097	(153, 42)	3.2 (10.3)	3.2 (10.6)	17,045

Table 2.7. Argonaut configuration parameters.

Blanking distance (m)	0.20
Maximum depth (m)	3.50
Cell size (m)	0.30
Number of cells	10
Collection time interval (s)	10

Figure 2.9. SonTek Argonaut unit. The ADCP is the lower instrument and the battery pack is the upper instrument. Cables are used to download data when the unit is removed from the water. The red discoloration is anti-fouling paint required for a prior salt-water deployment of the instrument.

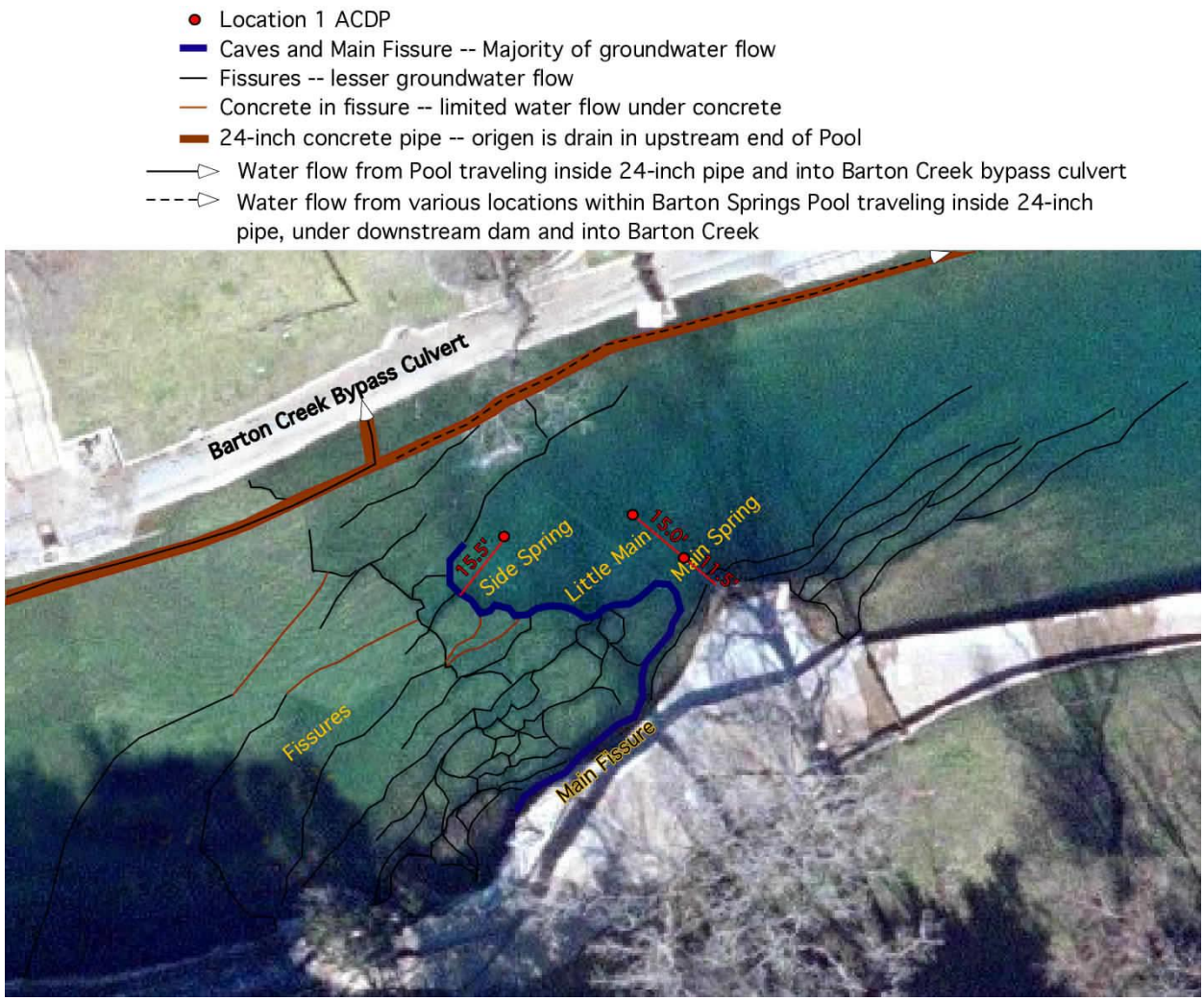

Figure 2.10. Fixed ADCP deployment locations (map courtesy of CoA, L. Dries, 2013).

2.7 Discharge Data

BSP discharge records[4] (Table 2.8) provide measured discharge values for each spillway, the bypass (which includes discharge from the 2 ft diameter pipe and from bypass leakage for discharge records prior to 2013), downstream of BSP for Barton Creek, and for Eliza and Old Mill Spring. The records were used to estimate the inflow

[4] Discharge records provided by J. Camp (2012), CoA Watershed Protection Department (WPD)

from Main Barton Spring by subtracting Eliza Spring's discharge from the downstream Barton Creek discharge. Measured discharge for the bypass included both discharge from the 2 ft diameter pipe along with discharge from BSP leaking into the bypass prior to discharge measurements collected in 2013, after which it just represented discharge from the pipe. The discharge measurements were used for comparison when adjusting the outlet coefficients, and will be used as a model calibration parameter (§4.2). Further discussion on the collection of discharge measurements is provided in Appendix C.

Table 2.8. Discharge data in cfs provided by J. Camp, CoA. Bypass leakage and Eliza Spring discharge were not available for 04/18/2011. For 2008, discharge data for 5 days when spillway 3 was closed and 7 days when spillways 2, 3, and 4 were closed were averaged separately.

Date	BSP Inflow	Spill way 1	Spill way 2	Spill way 3	Spill way 4	Spill way 5	Bypass Leakage and 2 ft diameter Pipe	Eliza Spring	Old Mill Spring
06/28/2013	16.5	1.98	0.61	0.76	0.78	4.59	6.40	1.70	0.60
08/06/2012	55	2.65	6.87	7.47	6.32	3.69	16.5	9.70	1.81
04/18/2011	31.5	0.51	2.44	2.32	2.33	0.78	n/a	n/a	0.31
Average for dates in 2008 with Spillway 3 Closed	25.2	1.02	3.54	n/a	3.51	1.42	6.58	3.12	0.18
Average for dates in 2008 with Spillway 2, 3, and 4 Closed	19.9	3.52	n/a	n/a	n/a	4.16	8.00	3.3	0.31

USGS gage 08155500[5] provides continuous discharge data for the Barton Springs complex. The discharge measurement is the combined discharge of Main, Eliza, and Old Mill Springs in the BSP area. Figure 2.11 shows the discharge at the USGS gage during the M9 survey, the Argonaut deployment, and during the CoA's discharge measurements in 2013. From the figure, it can be seen that BSP was experiencing low-flow conditions

[5] http://waterdata.usgs.gov/usa/nwis/uv?08155500

during all data collection surveys, since the discharge during data collection is much lower than the median 35-year daily discharge. To determine the discharge solely from BSP on data collection dates, an estimation for the allocation of contributing discharge to the USGS gage was found. The measured outflow from Eliza and Old Mill Spring was compared to the discharge from the USGS gage to find an average percentage of contributing flow for each spring, 12% and 1.3% for Eliza and Old Mill Spring, respectively (Table 2.9).

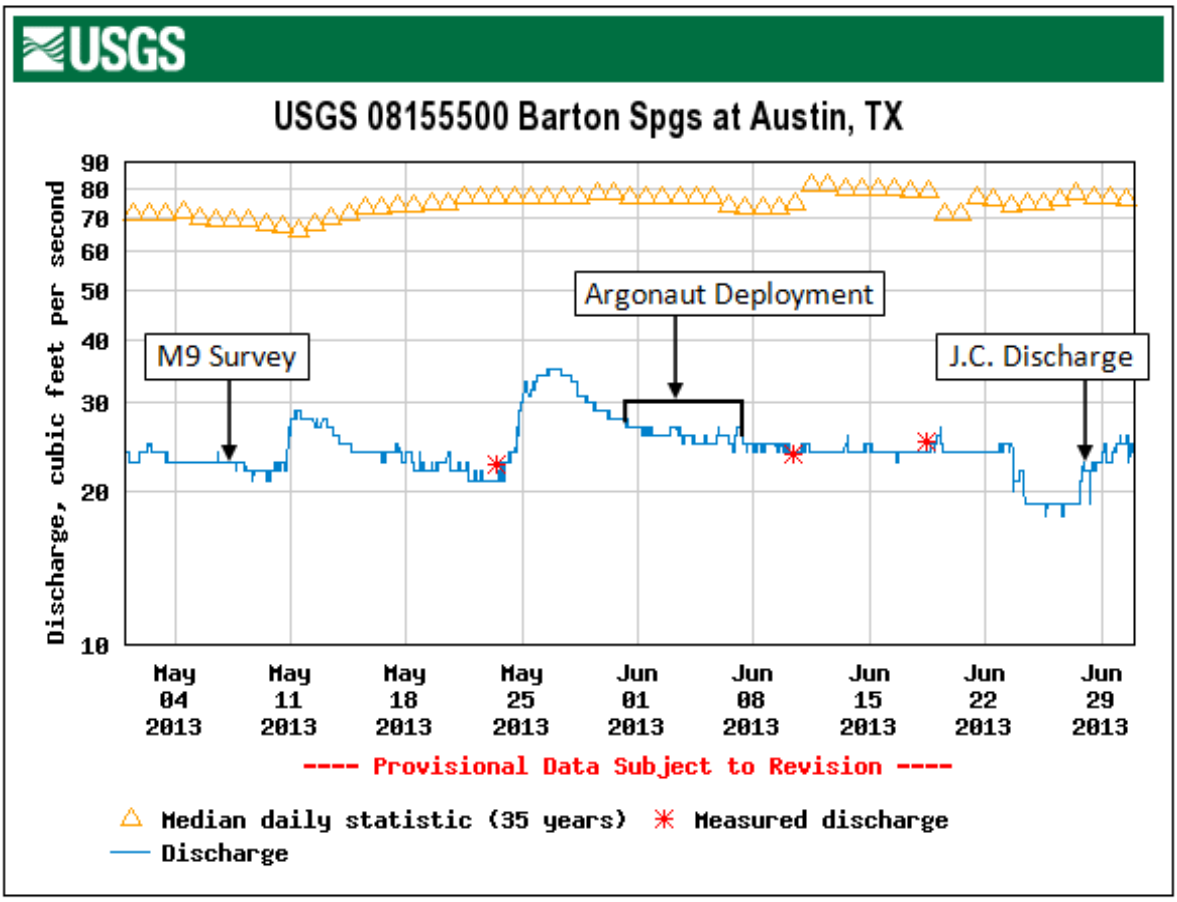

Figure 2.11. Discharge for USGS 08155500 for the data collection period.

Table 2.9. USGS gage discharge and spring discharge.

Date	Barton Springs Complex Discharge (08155500) (cfs)	Measured Eliza Spring Discharge (cfs)	Eliza Spring - Percent of USGS gage Flow	Measured Old Mill Spring Discharge (cfs)	Old Mill Spring - Percent of USGS gage Flow
06/12/2008	31	4.2	13.55	1.0	3.23
06/17/2008	29	3.4	11.72	0.7	2.41
06/26/2008	27	3.2	11.85	0.2	0.74
07/02/2008	26	3.1	11.92	0.0	0.00
07/10/2008	26	2.7	10.38	0.0	0.00
08/07/2008	23	3.2	13.91	0.0	0.00
08/14/2008	24	4.3	17.92	0.0	0.00
08/20/2008	29	3.1	10.69	1.1	3.79
08/29/2008	26	2.7	10.38	0.1	0.38
09/05/2008	25	3.1	12.40	0.1	0.40
09/19/2008	24	3.3	13.75	0.0	0.00
09/26/2008	23	3.3	14.35	0.5	2.17
08/06/2012	75	9.7	12.93	1.8	2.41
06/28/2013	23	1.7	7.39	0.6	2.61
Average Percentage of Flow	--	--	12.37	--	1.30

Chapter 3. The FREHD Model

3.1 Model Requirements

The description of the FREHD model is provided in §1.5.2. Running the BSP model requires MATLAB software, the FREHD source code, input files, analysis files, and an execution script. The input data required for the model are listed in Table 3.1.

Table 3.1. Input files for the FREHD model.

Input	Description
Bathymetry	Bathymetric map for the model area
Inflow	Inflow discharge and model cell locations for the inflow
Outflow: gates	Sizes and model cell locations for outflows modeled as gates
Outflow: pipes	Sizes and model cell locations for outflows modeled as pipes
Free surface	User specified free surface elevation
Layer	User specified model layer parameters

3.2 Model Input Data

3.2.1 Bathymetry

FREHD uses a raster grid of the bottom elevation to define the solution space. The creation of the raster grid is discussed in §2.4 and is illustrated Figure 2.4(C).

3.2.2 Spring Inflow

Since the bypass was created in the 1970s, the only inflow to BSP under normal-flow conditions is from spring inflow. The exact location of spring inflow varies, but is largely from Main Spring, which lies to the southwest of the diving board on the fissures[6]. Little Main and Side spring (locations shown in Figure 2.10) provide small

[6] L Dries, City of Austin, pers. comm. 2012.

contributions to the inflow. The model uniformly distributes the time-varying inflow rate over all of the user-specified inflow cells. The inflow cell locations were determined from aerial photography, bathymetry, and maps (such as Figure 2.10). Figure 3.1 shows spring inflow cell locations (in black) used in the model.

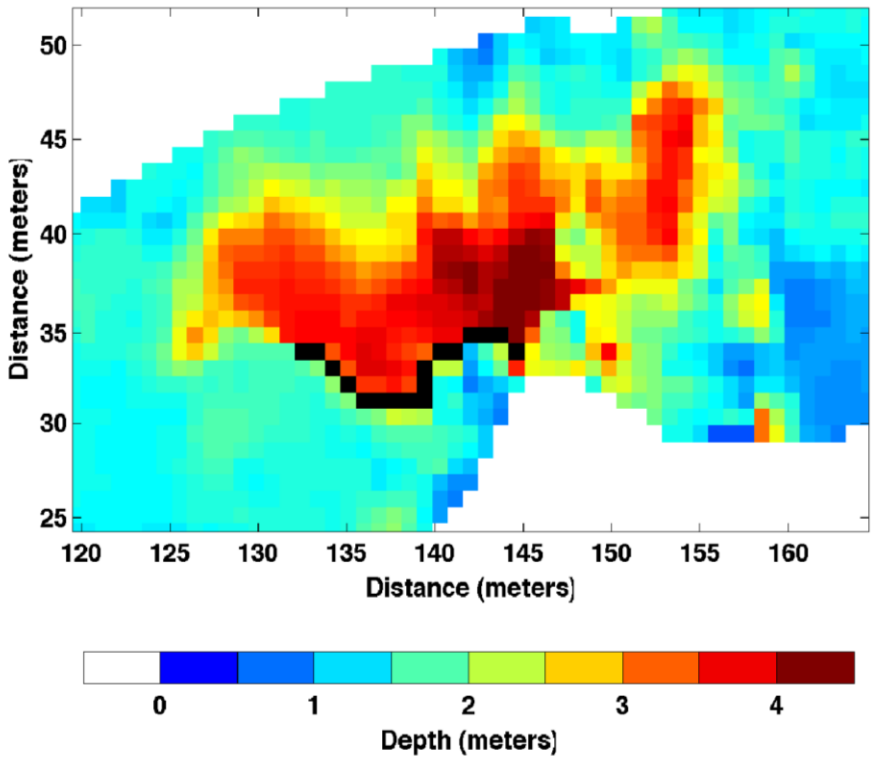

Figure 3.1. Inflow cells for the model, a magnified section of Figure 2.4 (C) near the BSP diving board.

3.2.3 Barton Springs Pool Outlets

The existing BSP outlets are described in §1.3. The four 2 x 2 ft gates in the downstream dam were not used for calibration since they are opened at most four times a year, and they were not opened during any data collection periods for this project. Outlets for BSP were modeled as either gates or pipes (Appendix E). The five spillways in the downstream dam were modeled as gates. In low-flow conditions, plates are placed in spillways 2, 3, and 4. The elevation of these plates for modeling purposes was determined based on provided information (Appendix E.1).

The horizontal layout for the 2 ft diameter pipe could not be precisely determined as the outlets have been modified over the life of BSP and documentation was unavailable. For this model, the pipe was modeled as a 0.61 m (2 ft) diameter pipe on the pool bottom with a total length of 104 meters, and an elevation change of -1.15 m between the pipe opening and where the pipe opens into the bypass. This setup provides a pipe bottom slope of 0.011. Hydraulic coefficients for the FREHD model for gate and pipe outlets control the water level within BSP and were adjusted to determine their effects on discharge (§4.2).

Chapter 4. Model Simulations and Comparisons

4.1 Overview

This section describes the use of the FREHD model with default settings and with an initial adjustment of the outlet coefficients. The outlet coefficients for the gates and pipes were adjusted (Appendix E) and the resulting modeled discharges were compared to measured discharge, and a sensitivity analysis was performed on the model's drag coefficient. The FREHD model was used to model the targeted discharges (low, average, and high-flow conditions) using the default settings (Table 4.1) and the adjusted outlet coefficients to visualize how inflow rates affect flow through BSP. The purpose of the initial outlet coefficient adjustment, sensitivity analysis, and simulations is to see how the model responds under the default settings, and to provide a framework for future modeling and calibration efforts.

Table 4.1 shows the model configuration parameters for the FREHD model. The model was run until it reached steady state, which was determined by finding when the total inflow and total volume have stabilized (Figure 4.1 and Figure 4.2). Total inflows should stabilize at 0 cfs, since spring inflow was treated as a positive inflow and outflows as negative inflows. Oscillations of the free surface are present in the initial timesteps as the surface water level equalizes with the inflows and outflows.

Table 4.1. Model configuration parameters.

Model Input	Value
Number of layers	20
Thickness of layers (m)	0.3
Free surface elevation (m)	4.81
Model grid cell size (m)	0.866
Bottom drag coefficient	0.02
Sidewall drag coefficient	0.01
Viscosity (X, Y, and Z; m^2/s)	$1*10^{-2}$
Timestep (s)	1
Gate coefficient	0.64
2 ft pipe coefficient	4.15
3.5 in pipe coefficient	6

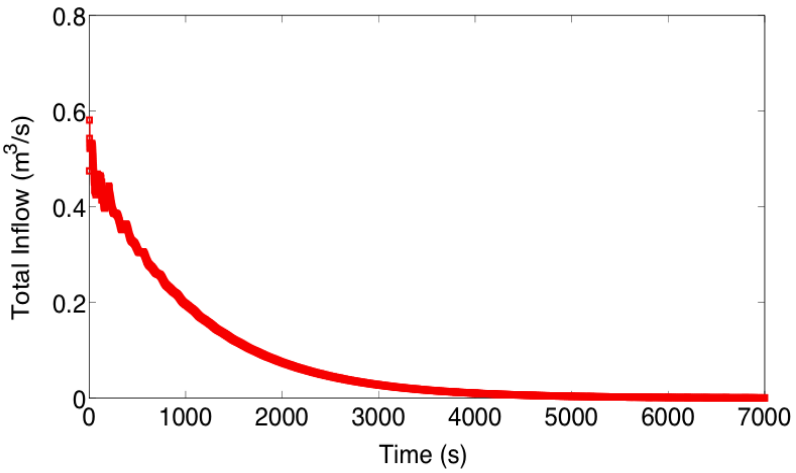

Figure 4.1. Total inflow reaching steady-state from the FREHD model.

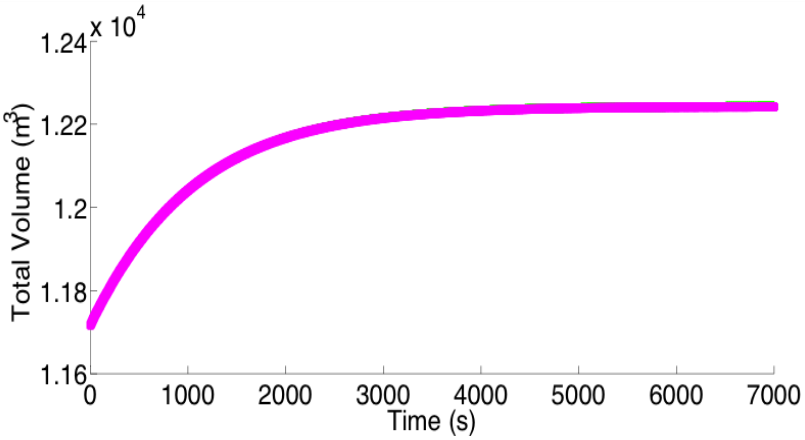

Figure 4.2. Total volume reaching steady-state from the FREHD model.

4.2 Outlet Coefficient Adjustment

The outlet coefficients for the FREHD model were varied and the resulting modeled steady-state outlet discharges were compared to the measured outlet discharges (§2.7). This was not a calibration, but was used to see how the model's outlet coefficients affected modeled discharge, and to provide a framework for future modeling. The gate coefficient and the pipe coefficients were jointly adjusted. Literature values for the discharge coefficient for open-channel flow through a rectangular gate range from 0.5 to 0.7 (Brater et al., 1996). After initial model runs, 0.64 was chosen as a reasonable value for the five spillways (Appendix E.1), and pipe coefficients were chosen as 4.2 and 6 for the 2 ft and 3.5 in. diameter pipe, respectively (Appendix E.2).

The modeled discharge was compared to measured discharge values (§2.7) for an average-flow conditions before bypass repair (Table 4.2), and for a low-flow condition after bypass repair (Table 4.3). Discharge data was not available for average-flow conditions after bypass repair, and this should be investigated in future modeling work.

For the average-flow condition before bypass repair, the modeled discharge seems to be overestimating the measured discharge. However, the measured discharge was prior to bypass repairs when large amounts of water continuously leaked from BSP into the bypass, meaning less water was available to discharge through the spillways. This can be seen by the large measured discharge for the 2 ft diameter pipe (which includes discharge from the pipe and from bypass leakage) in Table 4.2. For the low-flow condition, plates were placed in spillways 2, 3, and 4 to keep water levels in BSP at their normal levels. Appendix E.1 describes how these plates were modeled. Table 4.3 shows that the model

overestimates the discharge from spillways 1 through 4, but the total measured outflow is also 1.26 cfs less than the inflow. For future modeling purposes and calibration, more discharge measurements after the bypass repair and under a variety of flow conditions are required.

Table 4.2. Modeled discharge verses measured discharge under average-flow conditions before bypass repair. Note measured discharge for the 2 ft pipe includes discharge from the leaking bypass.

Inflow/Outflow	Model (cfs)	Measured discharge on August 6, 2012 (cfs)
Inflow Main BS	55.0	55.0
Spillway 1	6.71	2.65
Spillway 2	11.16	6.87
Spillway 3	11.16	7.47
Spillway 4	11.16	6.32
Spillway 5	6.75	3.69
2 Foot Pipe	6.67	16.5
3.5 Inch Pipe	0.62	n/a

Table 4.3. Modeled discharge versus measured discharge under low-flow conditions after bypass repair. Note n/a means the discharge measurement was not measured.

Inflow/Outflow	Model (cfs)	Measured discharge on June 28, 2013 (cfs)
Inflow Main BS	16.5	16.5
Spillway 1	4.59	2.00
Spillway 2	1.47	0.61
Spillway 3	1.47	0.76
Spillway 4	1.47	0.78
Spillways 5	4.59	4.59
2 Foot Pipe	6.56	6.40
3.5 Inch Pipe	0.61	n/a

4.3 Velocity-Depth Relationship

The relationship between velocity and depth provides insight into the hydrology of a system and can allow assumptions to be made for modeling purposes. The multi-cell temporal velocity profiles (§2.6) from the Argonaut unit were used to see how velocity changes with depth in BSP. Velocity profiles were averaged in 1-hour increments over the duration of the Argonaut deployment (Figure 4.3), and in 10-minute increments over the first hour of deployment (Figure 4.4) at every Argonaut location (Table 2.6) except location 1 since less than one hour of data was recorded. The time axis in Figure 4.3 represents the time elapsed since the Argonaut was deployed, and the locations move progressively further from the main spring inflow (a is the closest and c is the furthest away). For processing, the speed was calculated from the east and north component velocities, the mean (μ) and standard deviation (σ) was computed for speed at each cell over the averaging period, speeds outside of $\mu \pm \sigma$ were removed, and the mean was recomputed. Since the profile cells encompass a range of depths, the cell speed was plotted at the depth of the middle of the cell. The differing profile depths are due to the bathymetry at the locations, since the Argonaut recorded cell velocities from 0.2 to 3.2 m (Table 2.7) above the instrument.

The hour-averaged data shows that the speeds are relatively uniform, both temporally and throughout the profile. The data shows that the speed is generally greatest near the bottom due to the spring inflow in the area, and it appears that there might be small surface flows. These results show that using depth-averaged velocities is valid for this study of BSP.

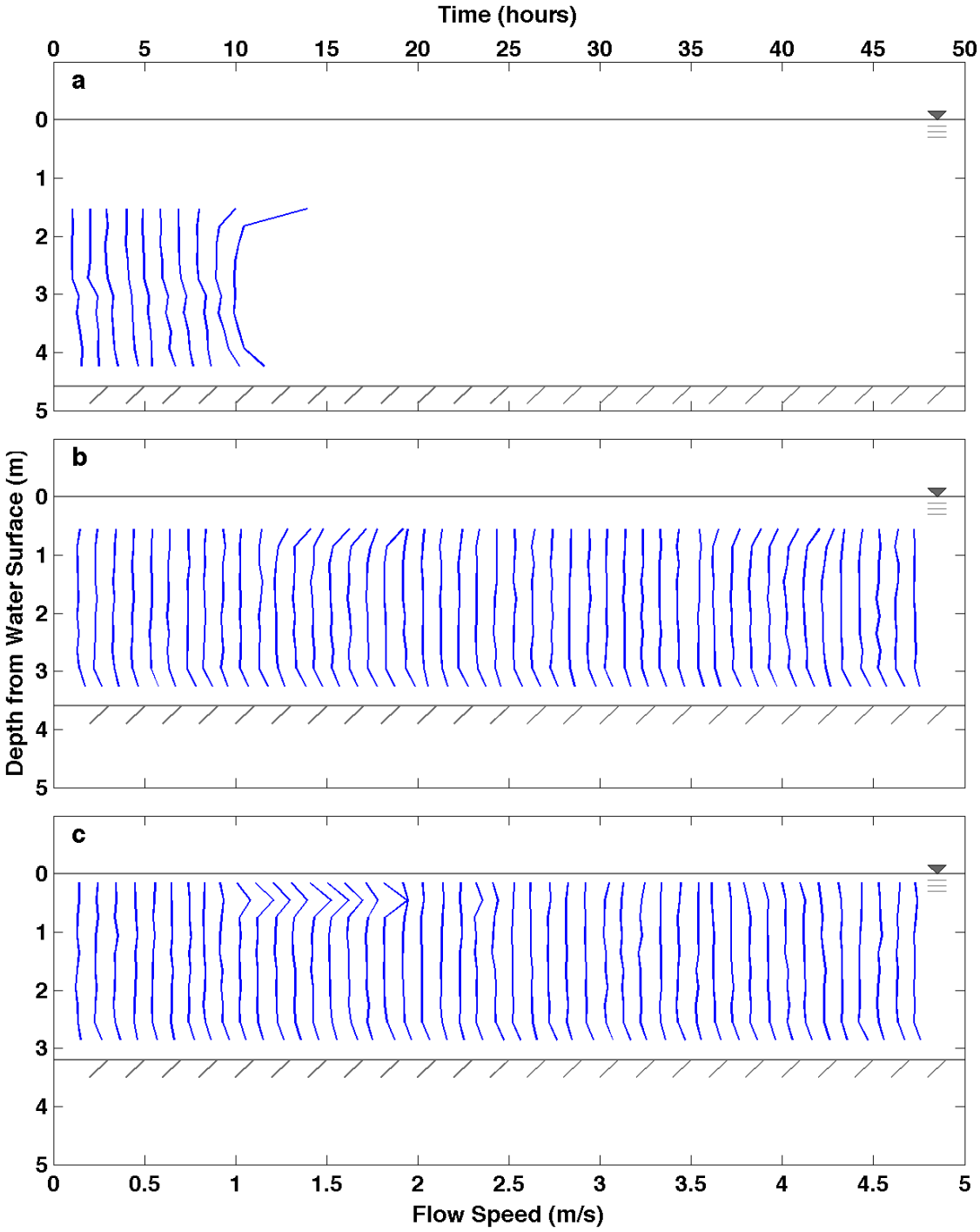

Figure 4.3. Hourly averaged flow speed profiles from the Argonaut ADCP in m/s incremented by 0.1 m/s over the course of ADCP deployment with water surface elevation and bathymetry plotted at Argonaut locations (a) 2, (b) 3, and (c) 4.

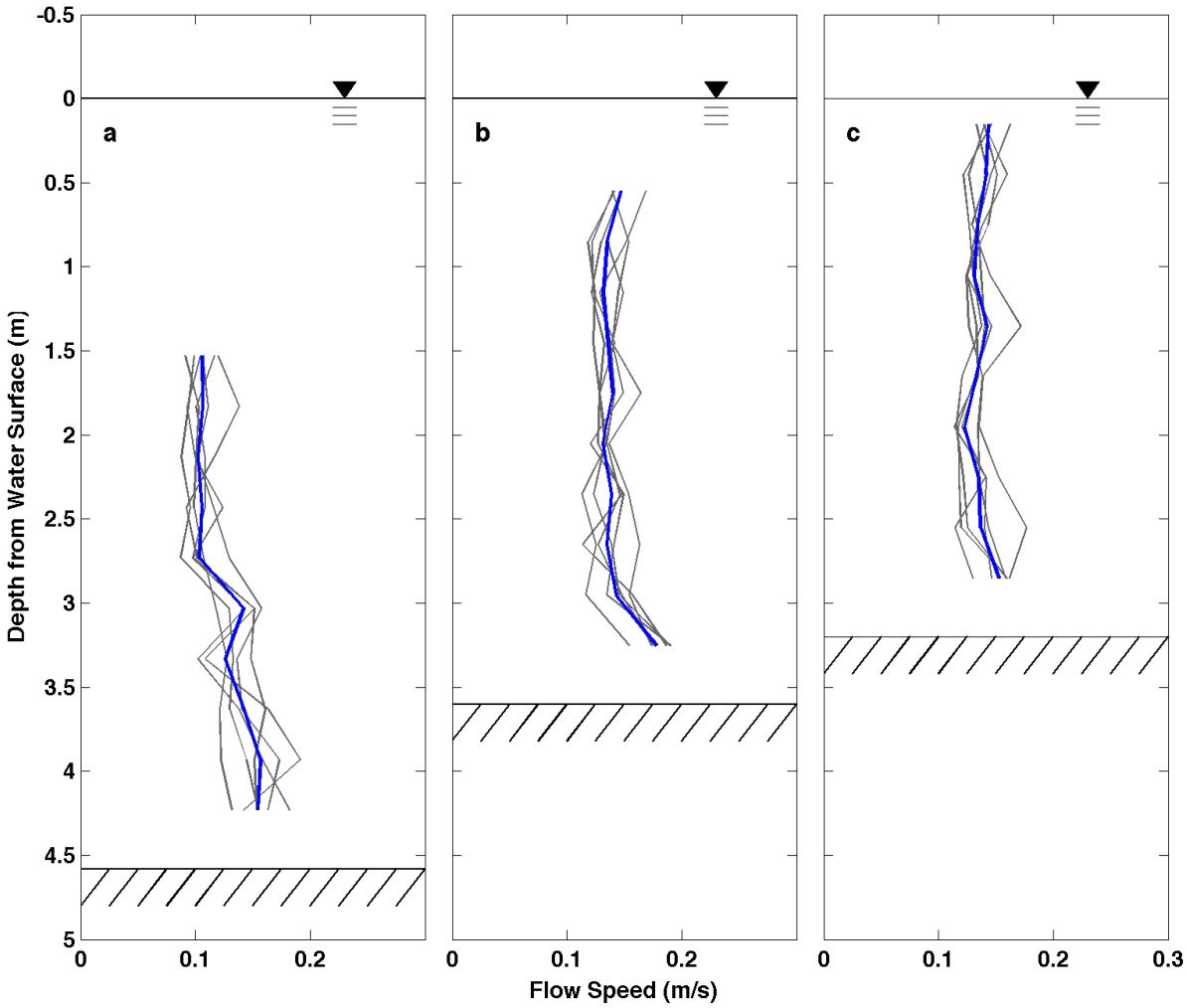

Figure 4.4. Ten-minute averaged flow speed profiles from the Argonaut ADCP in m/s for the first hour of ADCP deployment with water surface elevation and bathymetry plotted and with the first hour's mean plotted in blue at Argonaut locations (a) 2, (b) 3, and (c) 4.

4.4 Bottom Drag Coefficient Sensitivity Analysis

Drag coefficients provide a model of momentum losses through frictional resistance on the pool bottom, which includes effects of both bottom roughness and vegetation. In theory, the drag coefficient can range from zero to unity, with the extremes representing unrealistic conditions of no energy loss or complete energy loss. A range of 0.024 to 0.02 has been found for bays ranging from 0.6 m to 6.5 m (Wang et al., 1998), which encompasses the depths in BSP. The BSP model was tested for three different cases using uniform bottom drag coefficients of 0.002, 0.02, and 0.2 to test the sensitivity of the model to different drag coefficients.

The model for comparing the three drag coefficients was ran under an average-flow condition (modeled inflow was 1.54 m^3/s, 21.4 cfs) using the adjusted outlet coefficients and with the model parameters shown in Table 4.1 (except for the varying drag coefficient). Figure 4.5 shows modeled flow speed profiles resulting from three different bottom drag coefficients at Argonaut deployment locations 2, 3, and 4. Speed was calculated from the modeled east and north component velocities. The figure shows that the three drag coefficients provide nearly the same velocities. Since the bottom drag coefficient seemed to have little influence on the modeled velocities, a bottom drag coefficient of 0.02 was used for the present model results.

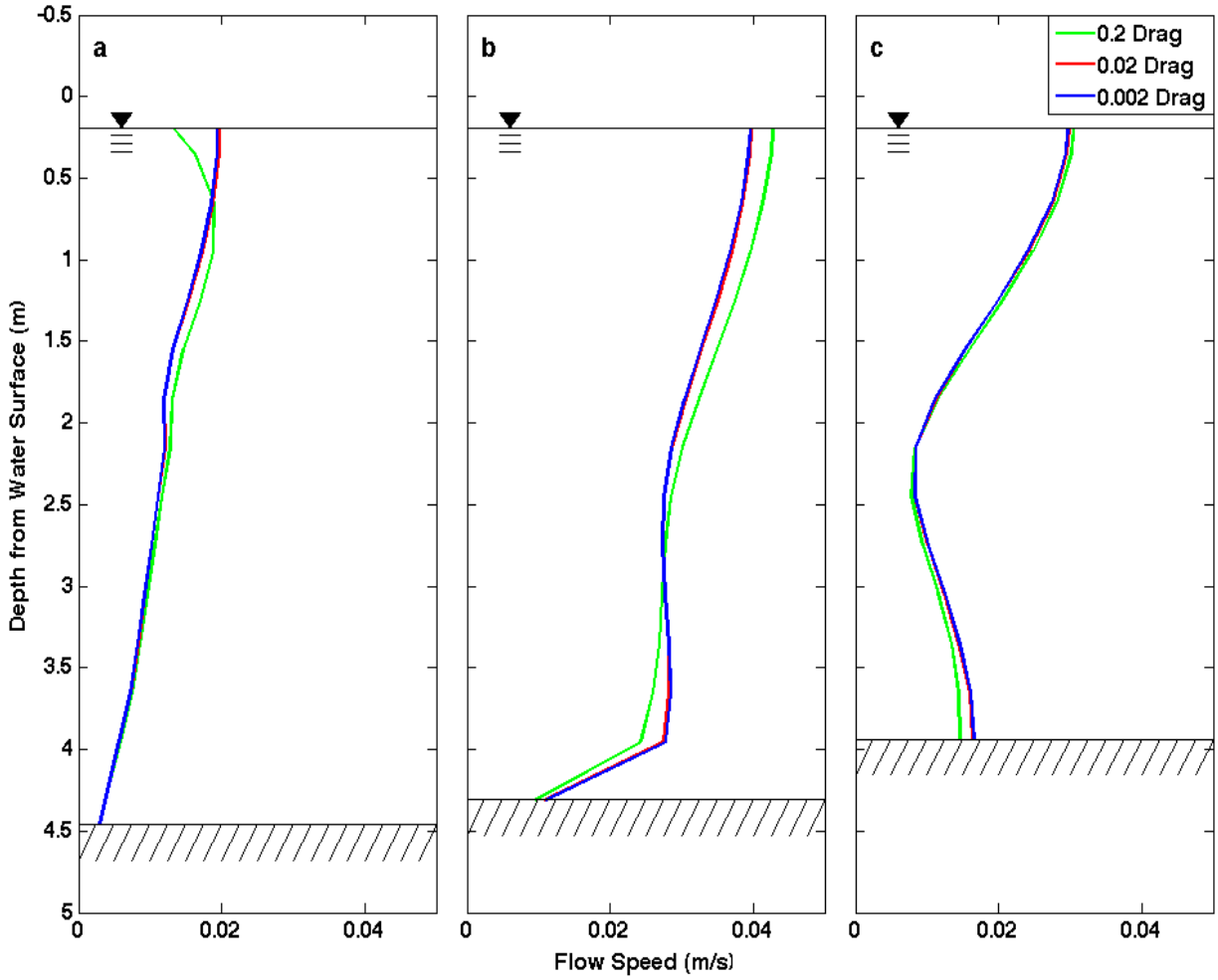

Figure 4.5. Modeled flow speeds in m/s resulting from three drag coefficients under average-flow conditions at (a) Argonaut location 2, (b) Argonaut location 3, and (c) Argonaut location 4.

4.5 Comparison between Modeled Velocities and Synoptic ADCP Data

Initial modeled speeds from the uncalibrated model using the default settings and the adjusted outlet coefficients were compared to the collected synoptic ADCP data to see how the default settings perform, and to test the sensitivity of the model. Modeled

and measured speeds were compared for all areas where ADCP data was collected. The model used an inflow of 0.54 m^3/s (19.07 cfs), with plates in the middle three spillways (Appendix E.1), and with the parameters shown in Table 4.1, since BSP was under low-flow conditions during the synoptic ADCP data survey. The inflow was estimated by determining the USGS discharge on May 9 and subtracting the estimated contribution of spring inflow to this discharge (§2.7). Speed profiles were depth-averaged, since §0 showed that this is a valid method for BSP. Since the ADCP data was very noisy, speeds for 5 x 5 grid cells (4.33 x 4.33 m) were averaged to get a single course velocity for the 25 cells.

Figure 4.6 shows the course averaged speeds for the ADCP and modeled flow speeds. Modeled speeds were much lower than collected ADCP velocities, indicating that under default conditions, the model does not produce the velocities recorded by the ADCP. However, since the model is uncalibrated and the synoptic ADCP survey was only performed once, it is not possible to say whether the ADCP is overestimating or the model is underestimating velocities. The magnitudes of the ADCP velocities seem unrealistically large, since the range of collected velocities would produce associated discharges many times greater than the actual inflow. The synoptic ADCP survey was only performed once, and occurred during low-flow conditions at BSP due to its closure for an extended period for bypass repairs. In addition, BSP experienced low-flow conditions during most of the duration of Phase 1 due to the Texas drought. In the future, more ADCP data should be collected under varying flow conditions to further validate the model, and to reduce the error due to noise from the ADCP.

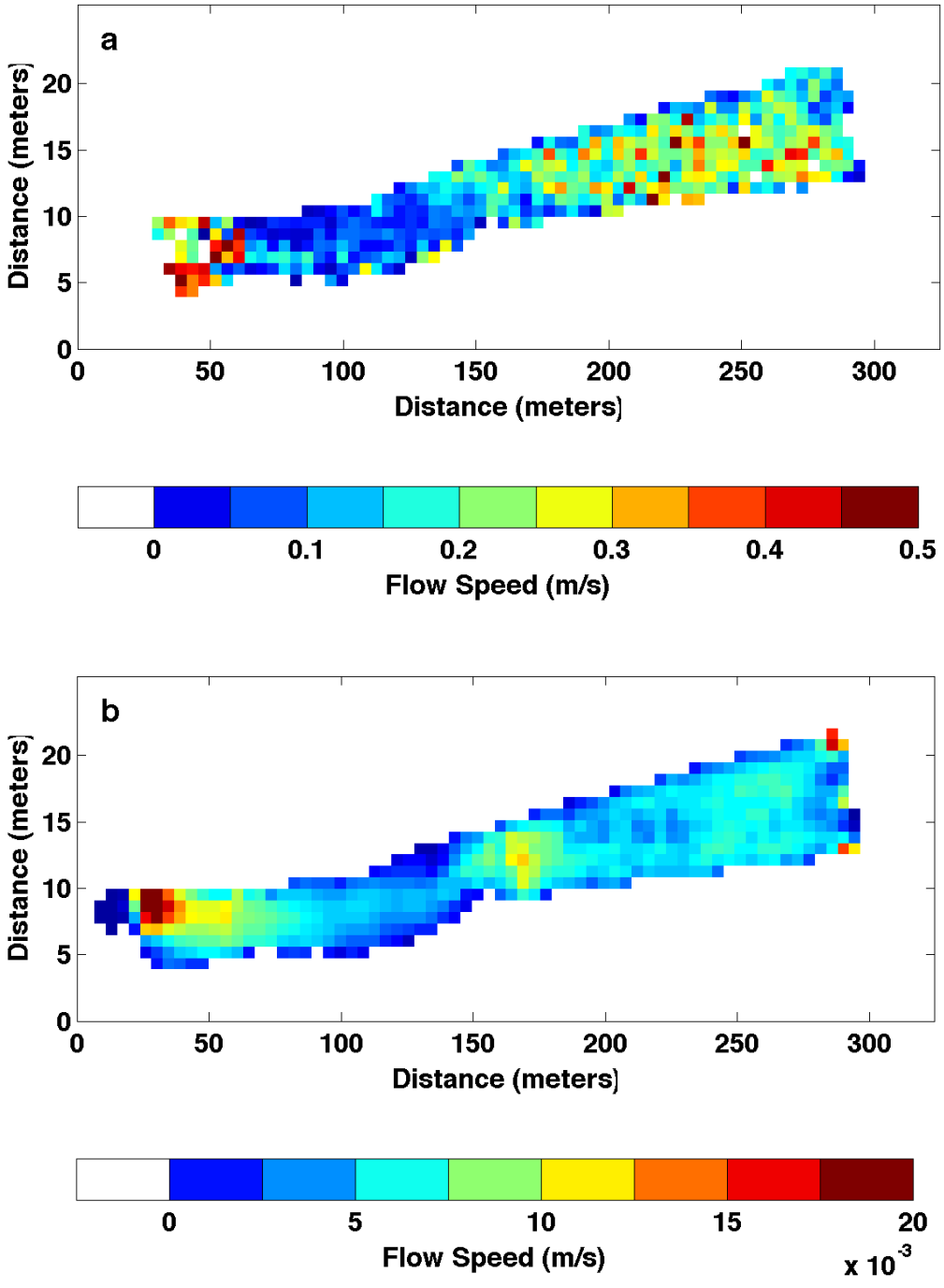

Figure 4.6. Flow speed averaged for 5 x 5 grid cells for: (a) the synoptic ADCP data; (b) the model.

4.6 Model Simulations for the Targeted Discharges

The three targeted discharges were low (10-30 cfs), average (40-70 cfs), and high-flow (85-100 cfs). The three discharges were modeled using the values shown in Table 4.1. Figure 4.7 shows the modeled flow speed in m/s in layer 16 (4.5 to 4.8 m above the zero reference point) under low-flow (a), average-flow (b), and high-flow (c) conditions.

The low-flow discharge condition was modeled with an inflow of 0.614 m^3/s (21.7 cfs), the average-flow condition was modeled with an inflow of 1.54 m^3/s (54.4 cfs), and the high-flow condition was modeled with an inflow of 2.6 m^3/s (91.8 cfs). Figure 4.7 shows that different inflows cause very different velocity conditions in BSP. Under low-flow conditions, velocities are low throughout BSP, with little variation in velocity magnitude in the upstream and downstream portions of BSP. This agrees with a previous study that found that under low discharge (25 to 30 cfs), velocity at the substrate in areas of BSP was less than the detection limit of the flow meter (Colucci, 2009). Under average-flow conditions, the downstream velocities are higher than for the low-flow conditions, and velocities in the upstream portion remain relatively unchanged, with several areas experiencing velocities near 0 m/s. Under the high-flow condition, the upstream and downstream portion of BSP have very different velocities, with several areas having velocities over 0.09 m/s, while most of the upstream portion has velocities below 0.02 m/s. These results show that an increase in inflow causes faster velocities in the downstream portion of BSP, but this is not reflected in the upstream portion.

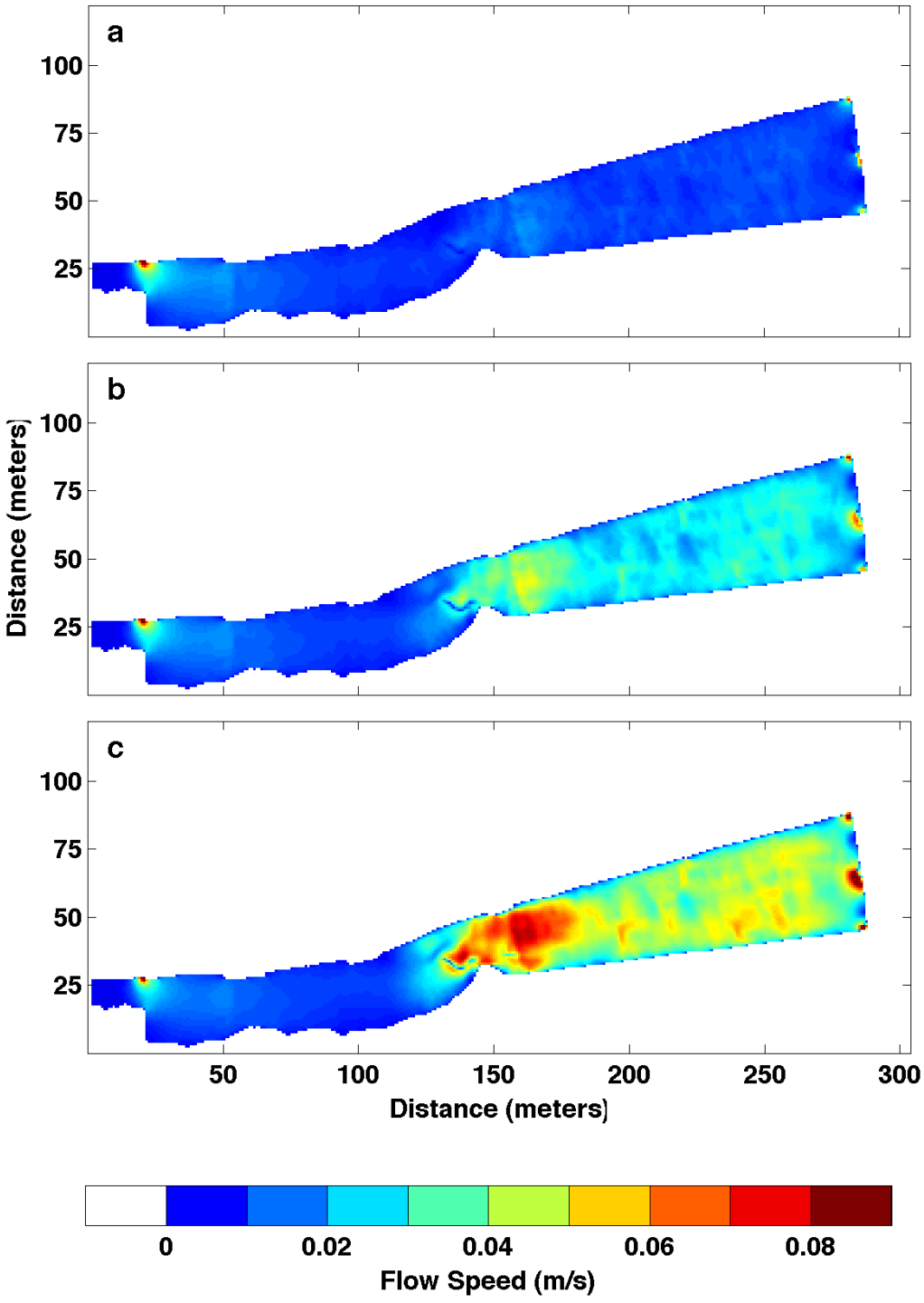

Figure 4.7. Modeled flow speed in m/s in model layer 16 for (a) low-flow, (b) average-flow, and (c) high-flow discharge conditions in BSP.

Chapter 5. Conclusions and Future Work

This report discusses the field data collection, model setup, and testing of the BSP hydrodynamic code under default settings. The collected field data included bathymetric data from sonar equipment, velocity data from two ADCP instruments, and discharge data. The model used was the FREHD version PC2v7g, developed at CRWR, UT. For this project, the model was run using default settings with some adjustments to see how the model performs. This report is part of a larger initiative to evaluate infrastructure issues in BSP.

Outlet coefficients were adjusted and the resulting modeled outlet discharges were compared to measured outlet discharges, a sensitivity analysis was performed to test how the model responds to different drag coefficients, and modeled velocities were compared to collected ADCP values from the synoptic survey. This comparison showed that the model underestimated velocities collected by the ADCP, indicating that future calibration of the model is required. One issue is that all of the field data collected after the bypass repair (discharge and both ADCP surveys) was collected under low-flow conditions. Discharge and ADCP data collection for average and high-flow should be targeted in the next phases of the project to correctly calibrate the model.

Modeling of the three targeted discharges showed that velocities in the upstream portion of BSP remained at relatively the same magnitude even as inflow increased dramatically, and as inflow increased, the difference between velocities in the upstream and downstream portion of the pool increased. This provides useful information to the

CoA when considering how to modify infrastructure to improve the flow regime of BSP. The effect that modifying infrastructure has on the flow through BSP will be further investigated in future phases of the project.

Appendix A Bathymetry

A.1 Wiring and Powering the Bathymetric Survey Unit

The wiring and powering of the HDS and StructureScan units was based on information in Lowrance's documentation (Lowrance 2011c), and from reading fishing message boards for installation ideas. Since most Lowrance equipment is for fishing purposes, boat batteries are usually used to power units. For this project, the battery needed to provide enough Amp-hours to power the units for a reasonable amount of time, while still being light enough to not sink the survey unit and small enough to fit in the bucket with the StructureScan. The battery also needed to be rechargeable, and needed to have terminals so the units could be easily connected and disconnected from the battery. The battery used was an 8Ah 12V UB1280 battery with F2 terminals.

Figure A.1 and Figure A.2 were used as references for wiring the units (Lowrance 2011c). Since NMEA devices were not used, the HDS data cable was not required, meaning only the power portion of that cable was used (3 out of the 8 wires, Figure A.1). The yellow wire in each unit's power cable is the accessory wake up line and allows units with the accessory wake up feature to be powered from one location. This cable was not used for this wiring. For both the StructureScan and the HDS, the red power cables were connected to a 10 Amp fuse and then to a terminal block, and the red wire from this block is connected to a spade connector, which is able to slide onto the F2 terminal of the battery. The black ground cables for both units were fashioned in the same manner except

they were not connected to fuses. The StructureScan and the HDS were connected using the ENET (Ethernet) cable.

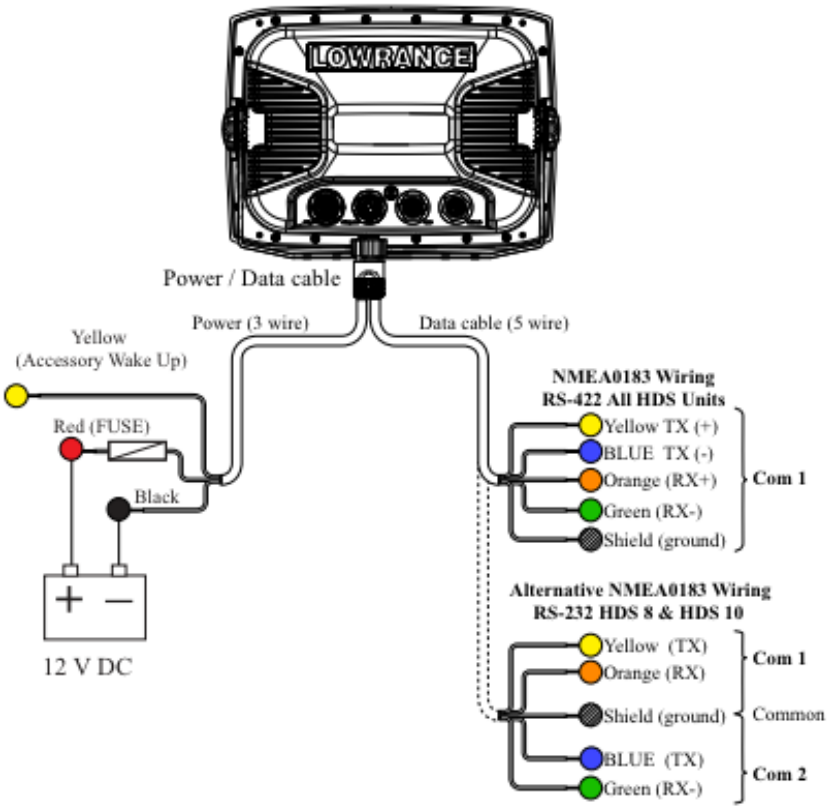

Figure A.1. Setup for the power/data cable of the HDS unit, which is similar to the power cable setup for the StructureScan unit.

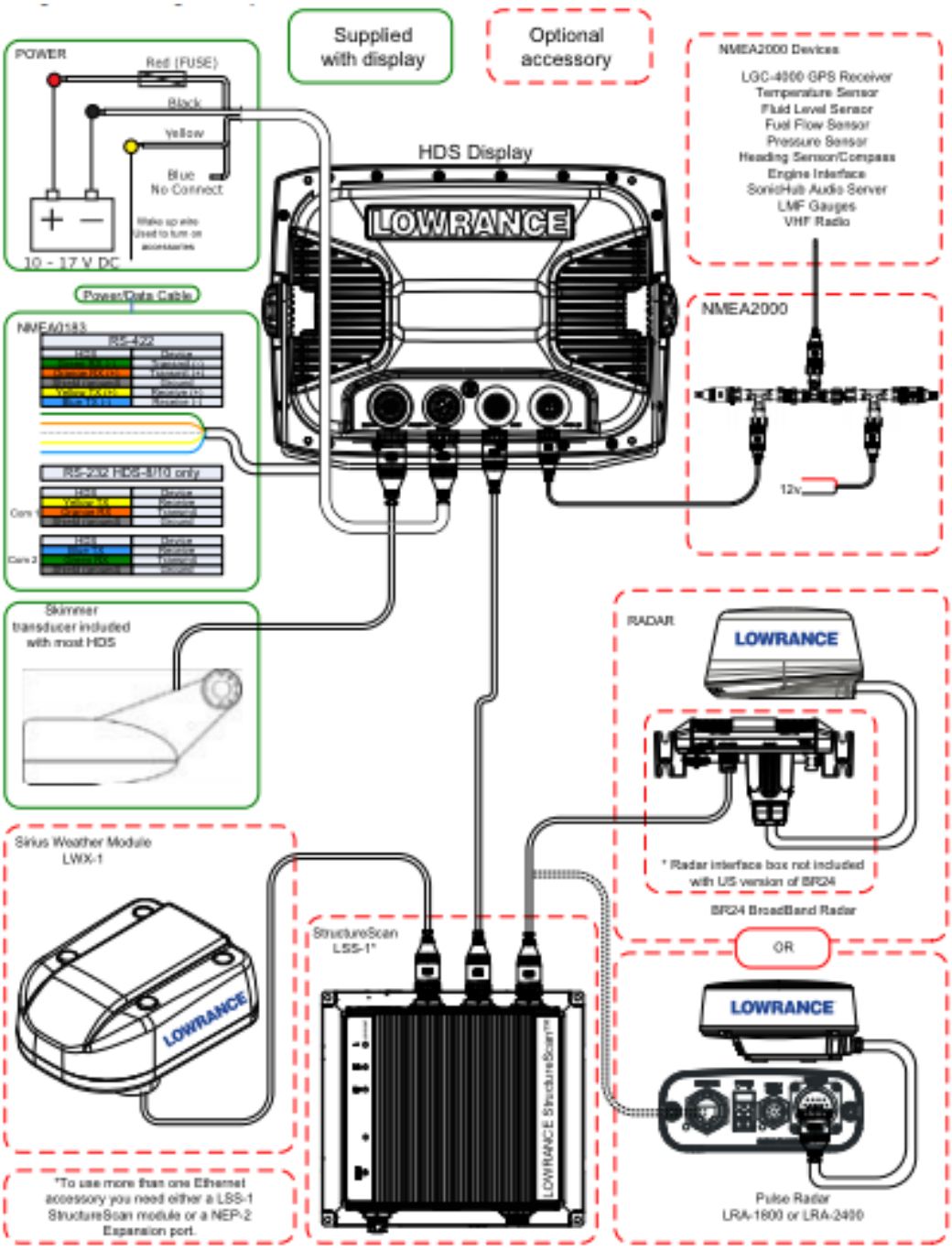

Figure A.2. Installation and wiring of the HDS unit to the StructureScan and battery. Note that this survey only used the HDS display and the StructureScan LSS-1, not the radars, NMEA devices, or the Serius Weather Module.

A.2 Steps to Process the Position-Depth Data

Section 2.4 discussed what was done to the position-depth data during processing and this section will discuss the steps on how the data processed. To process the data:

1. Open each recorded file in Sonar Log Viewer.
2. Convert the .sl2 files to .csv files in Sonar Log Viewer using the Output Chart Information utility.
3. Import the .csv files to Matlab and process the data as described below.
4. Create the boundary file for BSP (Appendix D.1).
5. Clip the data to the boundary and interpolate for areas without data.

Matlab scripts were created for processing bathymetric data but due to the length and number of scripts used for this report, they are not included. The scripts were used to perform the following tasks:

1. Separate the data into four datasets: all of the data, the HDS unit, the StructureScan downscan, and the StructureScan downscan.
2. Identify the unique positions (latitude and longitude combinations) for each dataset.
3. Create coordinate offsets (Appendix D.3).
4. Create a 3D matrix with dimensions equal to the latitude and longitude extents and assign each recorded depth to a level in the matrix.
5. Calculate a single mean for each grid cell (§2.4).

A.3 QA data for the bathymetric survey

QA transects were collected as a check of the repeatability of the bathymetric survey. Figure A.3 shows the approximate locations of the QA transects collected during the bathymetric survey. To collect the QA transect, the equipment was pulled back and forth along the QA line 2 to 3 times, and was recorded separately from the rest of the

data. QA bathymetric data was processed the same way as the other bathymetric data was (§2.4).

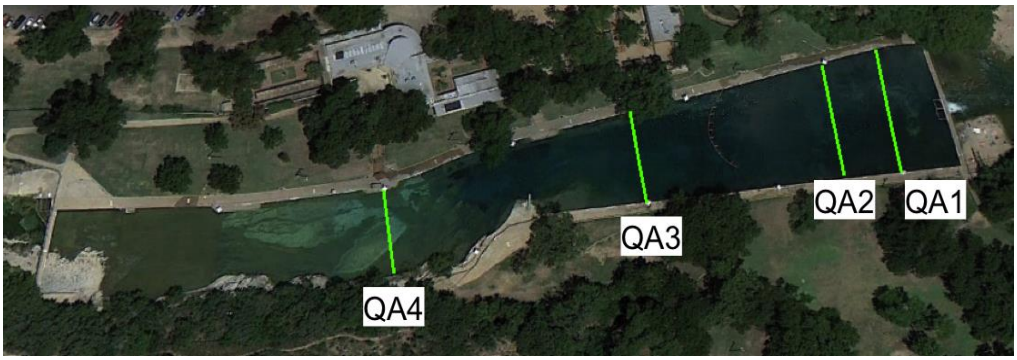

Figure A.3. Approximate location of the QA transects for bathymetric data.

To compare the processed QA transects with the other bathymetric data, the percent difference (Equation A.1) was found between processed the QA depths at each location on each night and the bathymetry used as a model input. A summary of the percent differences is provided in §2.4.

$$\text{Percent difference} = \left| \frac{\text{Main survey} - \text{QA}}{(\text{Main survey} - \text{QA})/2} \right| * 100\% \qquad \text{(A.1)}$$

A.4 Comparison of the Created Bathymetric Map

As part of the Barton Springs Master Plan, Survey and Mapping (SAM), Inc. performed a topographic survey of BSP, which included the floor of BSP, although at a more coarse scale than the bathymetric map developed in this study. Figure A.4 and Figure A.5 show the area near the diving board of BSP (the deepest portion of the pool) for the bathymetric map created for this study and from the survey by SAM, Inc. Although meters were used throughout this study, Figure A.4 is shown in elevation from

MSL in ft for easier comparison to Figure A.5. The figures show that the elevation of the deepest portion of BSP from both studies agrees (about 417 ft), and the elevation for the fault to the northwest of the diving board agrees (about 427 ft). The depth pattern can also be confirmed by looking at a high-quality photograph provided by the Bureau of Economic Geology (Figure A.6).

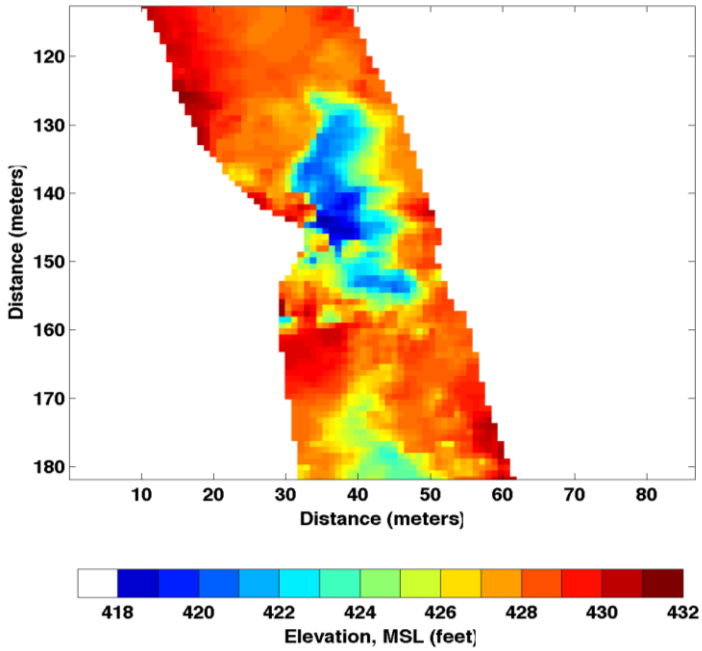

Figure A.4. Bathymetric map created for this study in elevation from MSL (ft), magnified for the area near the diving board of BSP.

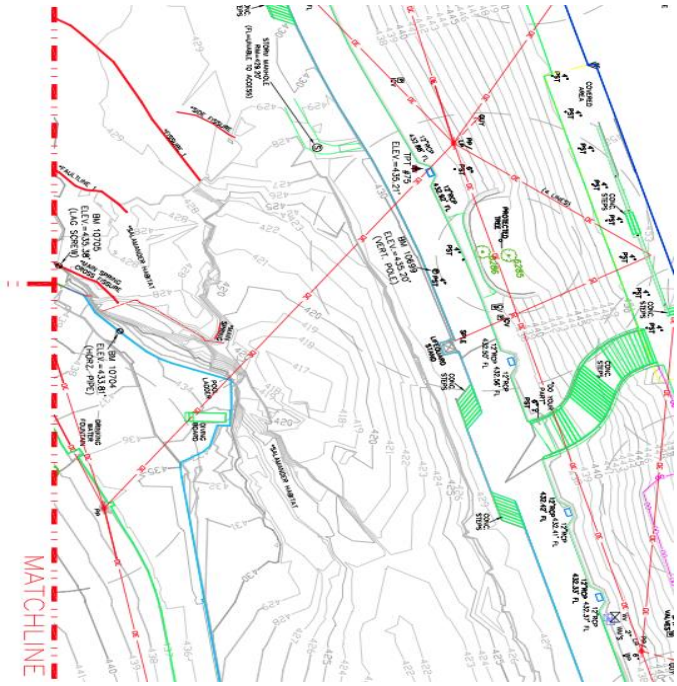

Figure A.5. Topographic survey completed by SAM, Inc., sheet 5, magnified for the area near the diving board of BSP.

Figure A.6. Aerial photograph provided by the Bureau of Economic Geology, magnified to the area near the diving board of BSP.

Appendix B ADCP data

B.1 Data Collection Steps for the Synoptic Velocity Data

Section 2.5 provides an overview of the synoptic velocity data collected using a SonTek/YSI M9 ADCP. The following lists the procedure for data collection using the M9 ADCP. The list was adapted from one created by David Christiansen for use of the ADCP mounted on a boat for a velocity survey of Galveston Bay. Note that RiverSurveyor setup followed the same steps except for slight differences in steps 1 and 2 in Collecting Data.

Before Data Collection

1. Attach the ADCP unit to the provided mount, tightening all 4 thumbscrews until they no longer move. Be sure the communication cable connection is lined up with the hole in the side of the mount
2. Connect the ADCP to the PCM unit using the waterproof cable protruding from the small Pelican case.
3. Open the small Pelican case.
4. Place a battery pack from the HydroSurveyor case into the PCM unit
5. Ensure the PCM unit is connected to the GPS unit with the coaxial cable
6. Push the large button on the PCM unit (it should turn green)
7. Do not yet close the Pelican case
8. Turn on the PC equipped with HydroSurveyor
9. Ensure the Bluetooth Adapter is connected using both USB cables
10. Open HydroSurveyor on PC
11. Select either “New project” or “Open project,” depending on the situation (If starting a new project, see the HydroSurveyor User’s Manual (SonTek 2012a)

for setup instructions. It can be accessed through HydroSurveyor in top left corner of screen.)

12. To connect to devices, select "Connect Devices" and click "Auto Detect" in the window that appears
13. After a few seconds, both the "HydroSurveyor" and "Auxiliary HydroSurveyor GPS" should connect. If they don't, check the PCM unit. The "GPS" and "Radio" lights should be green. If they're not, push the large button on the PCM unit, wait a few seconds, and push it again. Generally, if the PCM unit has been turned on at least 5 min. before attempting to connect to the units using the PC, the "Auto Detect" works.
14. Close the Pelican case and attach it to the back of the kayak.

Compass Calibration

1. See Section 9.1 in the HydroSurveyor User's Manual. Involves paddling the kayak in a circle with tilting it back and forth for a set period.

Collecting Data

1. To begin collecting data, press the "Start" button in the HydroSurveyor software.
2. To stop collecting data, push the "Stop" button in the HydroSurveyor software.
3. If stopping data collection for an extended period, turn off the PCM unit and remove the battery pack, disconnect the ADCP from the PCM unit and remove the ADCP from the mount and place it in the HydroSurveyor case.

B.2 Steps to Process the Synoptic Velocity Data

SonTek M9 data was viewed in RiverSurveyor (SonTek 2011) for Deployment 1 and HydroSurveyor (SonTek 2012b) for Deployment 2. For RiverSurveyor, only two steps were required for processing the data:

1. Output the session data as .mat files using processing toolbox to export to Matlab.
2. Run script_ADCPImport_03222013 making sure to specify the file directory and the exported session names.

Both RiverSurveyor and HydroSurveyor data were processed in Matlab. RiverSurveyor data can be exported to .mat files by session using the processing toolbox. The process for HydroSurveyor was more complicated due to differences in data output and an error in the software that does not allow some of the exported files to be read in Matlab. Matlab scripts were used for processing the data but are not shown due to space constraints. The steps for processing the HydroSurveyor data are:

1. Output each file as a .csv file.
2. Open the file as a comma delimited file in excel.
3. Delete everything but east, north, up, and error cell data (cells A:AF) and save this file as CellData.
4. Reopen the original .csv file and now delete the cell data (cells AG:LT) and save this file as CellInfo.
5. Import the CellData (as a matrix) and CellInfo (as a column vector) files into Matlab.
6. Repeat steps 2 through 4 for each session.
7. Organize the data into a 3D matrix, where the length is every velocity profile collected during the session, the width is the number of cells in the velocity profile, and the third dimension is: east (1), north (2), up (3), and the velocity error (4).
8. Combine all of the collected sessions and convert the coordinates to the corresponding offset Mercator Meter coordinates (Appendix D.2 and D.3).
9. Adjust the velocity profile cell size so that cells for all profiles are the same size.

10. Combine velocity profiles at the same unique coordinate, compute the mean velocity for each cell in the profile if there is more than one profile at a location.
11. Compute the mean for each profile at a user-specified layer height (necessary when comparing modeled cell velocities to ADCP cell velocities).

The SonTek M9 data is expressed as velocity profiles broken into cells of a certain size (defined as the cell size) based on the resolution at that location, and with the distance from the top of the water surface to the start of the first cell at each location (defined as the cell start). One issue with the initial SonTek M9 data is that the velocities for the same cell number do not necessarily correspond to velocities at the same depth among profiles, due to differences in resolution between profiles (which results in different cell start depths and cell sizes). This is adjusted for by setting a minimum cell size (set as 0.01 m for this survey due to the fine-resolution of BSP) and making all velocity profiles have a cell size equal to this set minimum. For instance if a profile had a cell start of 0.06 m and a cell size of 0.02 m, the code would create six empty cells before filling in the first velocity, then would enter the first recorded velocity in cells 7 and 8 since each cell size is 0.01 m. If more than one velocity profile exists at each unique location, the cell velocities were averaged, creating a single averaged velocity profile at each location with a cell size of the set minimum cell size. The data was also processed into user specified layer heights, where velocities for the layer were found by averaging velocities for the cells within each layer.

B.3 Data Collection of the Temporally-Evolving Velocity Data

Section 2.6 provides an overview of the temporally-evolving velocity data using a SonTek Argonaut ADCP unit. The Argonaut system includes an external battery pack, internal recorder, compass/tilt sensor, pressure, and temperature sensors (SonTek, 2004). The Argonaut collects velocity profiles in two formats: MultiCell, where velocity profiles are recorded, and as a dynamic velocity, where a single depth-averaged velocity is recorded. The Argonaut's dynamic velocity cell automatically adjusts for water height using the instrument's pressure sensor. This value represents a single, integrated velocity at the location over time. The pressure sensor also provided an easy way to see if and when the Argonaut was moved, as the pressure rapidly went from stable to sporadic at these times. The software ViewArgonuat (SonTek 2010) is used to setup deployments, to transfer the recorded data from the Argonaut to a PC, and to process the recorded data.

B.4 Processing the Temporally-Evolving Velocity Data

Data exported from the ViewArgonaut software can be viewed in a text editing software. Several files are exported during this process. The files that were used were the .ctl file that has the data collection parameters (such as the cell size and blanking distance), .vel that has the cell velocity data, and .dat that has the dynamic velocity data and parameters such as temperature and pressure. These files were copied from the text edit software into excel (formatted as space delimited), and then imported into Matlab.

Appendix C Discharge Data

Discharge data was provided for 13 days in 2008, one day each in 2011, 2012, and 2013. Discharge measured on June 28, 2013 was the only discharge data after the bypass repair was completed. Justin Camp from the City of Austin, Watershed Protection Department, provided the data along with the following methodology. Prior to 2010, all of the discharge measurements were collected using a Marsh-McBirney Flo-Mate Model 2000 Portable Flowmeter; since 2010, discharge measurements in the bypass and downstream of the dam were collected using a SonTek FlowTracker Handheld ADV. Discharge was measured in the spillways by dividing each spillway into at least four "cells", measuring the velocity in each cell, multiplying the velocity by the area of the cell (the width of the cell and the water depth), and correcting based on abnormalities in that cell (for example, chipped concrete). The discharge from these cells is then summed to provide a total discharge for each spillway. Figure C.1 shows the discharge measurement procedure for the spillways (A), and for the bypass and downstream of BSP (B).

Figure C.1. Discharge measurement procedure for (A) the spillways and (B) the bypass and downstream of BSP.

Appendix D Viewing the Collected Data

D.1 Creating the Boundary of BSP

The boundary of BSP was defined as the area where the water met the concrete and rock, and was created by outlining BSP in Google Earth. The boundary was saved as a .kml file and the coordinates for the file are in the World Geodetic Coordinate System (WGS 84). The created BSP boundary was imported into ArcGIS to verify on another aerial image that the created boundary aligned with the actual boundary of BSP. The function kml_shapefile, found on the Matlab file exchange, was used to bring the created kml Google Earth file for the boundary of BSP into Matlab (Toomey, 2010).

D.2 Converting Between Mercator Meters and WGS 84

The boundary coordinates were converted to Mercator Meter coordinates using an excel macros written by King and Zheng (2004) from Colby College and modified for use with Matlab. The macros defined the following variables:

```
RadToDeg = 57.29578;
DegToRad = 0.017453;
b = 6356752;
Pi = 3.141593;
Half_Pi = Pi / 2;
```

To convert longitude from WGS 84 to Mercator Meters, the following equation was used:

$$\text{GeoToMerX} = \text{GeoX} * \text{DegToRad} * \text{b} \tag{D.2}$$

where GeoToMerX is the longitude in Mercator Meters, GeoX is the longitude in WGS 84, and the variables are defined above. To convert latitude from WGS 84 to Mercator Meters, the following equation was used:

$$\text{GeoToMerY} = b*[\log(\tan(\text{GeoY}*\text{DegToRad} + \text{Half\_Pi})*0.5)] \quad \text{(D.3)}$$

where GeoToMerY is the latitude in Mercator Meters, GeoY is the latitude in WGS 84, and the variables are defined above.

To convert longitude from Mercator Meters back to WGS 84, the following equation was used:

$$\text{GeoX} = (\text{GeoToMerX}*\text{RadToDeg}) / b \quad \text{(D.4)}$$

To convert latitude from Mercator Meters back to WGS 84, the following equation was used:

$$\text{GeoY} = \text{RadToDeg}*\left(2*\text{a tan}\left(\exp\left(\text{GeoToMeryY} / b\right)\right) - \text{Half\_Pi}\right) \quad \text{(D.5)}$$

D.3 Offsetting the Mercator Meter Latitudes and Longitudes

Offsets were created so that the grid size would range from 1 to the maximum latitude and longitude, rather than having large numbered grid cells. The offset was determined by subtracting one from the minimum recorded latitude and longitude from the bathymetric data. The longitude offset for Mercator Meters is -10847476 and the original offset for latitude was 3525584. However, the bathymetric grid was adjusted after clipping out data and was shifted in the Y direction by 9 cells. Therefore, the actual latitude offset is 3525593. Subtracting these values from coordinates in Mercator Meters gives the offset locations, which corresponds to the cell number in the model.

D.4 Determining the Model Grid Cell Size

The model grid was created using the offset Mercator Meter coordinates. The cell size for the grid was therefore the distance between the each Mercator Meter recording point. Six locations were used to determine the distance between Mercator Meter coordinates (Table D.1, Figure D.1). Distances from locations 1 to 2, 3 to 4, and 5 to 6 were found to determine cell size in the x direction, and distances from locations 1 to 3, 2 to 4, 3 to 5, and 4 to 6 were used to determine the cell size in the y direction. Distances were found using the Haversine formula. All distances were equal to 0.866 m, meaning the model's grid cell size is 0.866 x 0.866 m.

Table D.1. Coordinates for 6 data points used for determining the model cell size in model cell, Mercator Meter, and WGS coordinates.

Location	Model Cell	Longitude Mercator Meters	Latitude Mercator Meters	Longitude WGS 84	Latitude WGS 84
1	(196,56)	-10847280	3525649	-97.7705803967856	30.2638423284267
2	(197,56)	-10847279	3525649	-97.7705713834126	30.2638423284267
3	(196,55)	-10847280	3525648	-97.7705803967856	30.2638345434520
4	(197,55)	-10847279	3525648	-97.7705713834126	30.2638345434520
5	(196,54)	-10847280	3525647	-97.7705803967856	30.2638267584767
6	(197,54)	-10847279	3525647	-97.7705713834126	30.2638267584767

Figure D.1. The 6 locations used for determining model grid cell size mapped in Google Earth.

Appendix E Modeling the Gates and Pipes

E.1 Gates

The five spillways in the downstream dam were modeled as gates. The equation used for gate modeling was the equation for orifices under low heads (Brater, King, Lindell, and Wei, 1996), and discharge can be computed by

$$Q_t = \frac{2}{3} C^* L \sqrt{2g} \left(h_2^{3/2} - h_1^{3/2} \right) \tag{E.1}$$

where L is the orifice (gate) width, and h1 and h2 are shown in Figure E.1. The above equation is the theoretical formula with an added C coefficient. From literature values, expected coefficients range from about 0.55 to 0.70. An initial value of 0.6 was chosen when beginning the rough calibration of the outlet coefficients and this was varied until discharge out of the spillways seemed realistic and pool volume stabilized. The C coefficient can be backcalculated using measured discharge values, but the calculated coefficients ranged from 0.1 to 0.6, so the above method was used instead for finding C. In the case of spillways, h_1 would be zero for average-flow conditions. Instead of specifying h_2 values in the code, the bottom elevation (from the zero reference point) of the gate is specified, along with the gate height. This was done because h changes as water elevation in BSP changes, and this allows for h values to be calculated for each timestep. Figure E.2 shows the setup and application of the above equation for modeling the spillways. The same values would be inputted for gates, but the water surface would

be above the top of the gate (the model would determine this based on the water elevation calculated by the model).

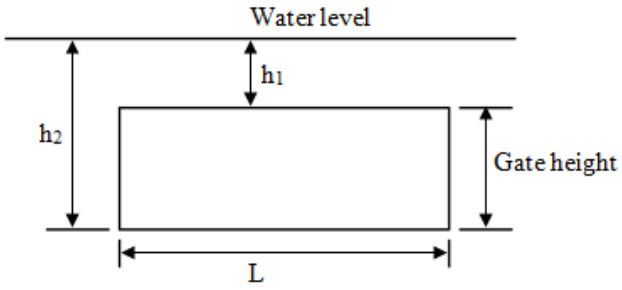

Figure E.1. Picture of gate setup based on equation D.1.

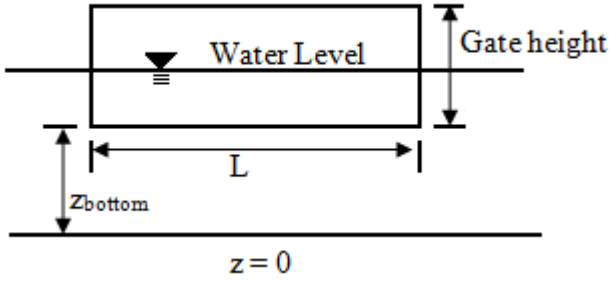

Figure E.2. Picture of gate setup for modeling spillways.

In low-flow conditions, plates are placed in spillways 2, 3, and 4. The z_{bottom} for the spillways with plates was determined by provided information on discharge from the spillways[7]. Data showed that the depth of water over the spillways was 0.12 ft (0.0366 m), which was subtracted from the free surface elevation of 4.81 m. The z_{bottom} for the plated spillways was modeled as 4.77 m and was 4.65 m for the open spillways.

E.2 Pipes

Two pipes were used for the initial modeling of BSP, the 3.5 in. pipe in the downstream dam and the 2 ft pipe near the upstream dam. The pipes proved more

[7] Provided by J. Camp (2012), CoA Watershed Protection Department (WPD)

difficult to model than the spillways. The current model is limited by the fact that pipes cannot cross cell layers due to the setup of the outlet code. For model calibration, the layer height was set to 0.3 m, meaning the 2 ft diameter pipe was modeled as a 0.29 m (0.95 ft) pipe in order for it to not cross a layer boundary.

The Darcy-Wiesbach equation, shown below, was used to find pipe flow:

$$Q = \left(\frac{2gA^2H}{K} \right)^{1/2} \tag{E.2}$$

where A is the area of the pipe, H is the water level, K is the coefficient for all friction and entrance and exit losses at the submerged entrance flow, and g is gravity. Figure E.3 shows the model inputs required for pipes, where $z_{inside,center}$ is the elevation to center of the entrance of the pipe, $z_{outside,center}$ is the elevation to the center of the exit of the pipe, d is the diameter of the pipe, and H is the water elevation that the model calculates for each time step. The model requires inputs for K for each pipe. Initial estimates for these coefficients were found using measured pipe parameters and discharge values. K for the above equation was found using the below equation:

$$K = f\left(\frac{L}{d} \right) + K_e \tag{E.3}$$

where f is the friction factor found using the Swamee and Jain equation (Swamee and Jain, 1976), L is the length of the pipe, d is the diameter of the pipe, and K_e is the entrance and exit losses and was assumed to be 1.5. The Swamee and Jain equation is:

$$f = \frac{1.325}{\left[\ln\left(\varepsilon/3.7D + 5.74/Re^{0.9} \right) \right]^2} \tag{E.4}$$

where ε is the roughness size for pipes, D is the diameter of the pipe, and Re is the Reynolds number. Re was estimated for both pipes using the equation below:

$$\mathrm{Re} = \frac{vD}{\nu} \tag{E.5}$$

where v is the velocity, D is the diameter of the pipe, and υ is viscosity.

The above process describes how K values can be found for pipes. K values for both pipes were calculated and were used as the input coefficients. For both pipes, v was estimated by dividing the expected discharge from each pipe (a measurement that could be measured with a flowtracker but this data was not available), by the area of the pipe. The ε value was estimated as 0.005 m for rough concrete from Table 6.1 in (Brater, King, Lindell, & Wei, 1996), and υ was assumed to be $0.963*10^{-6}$ m^2/s based on 22°C (the temperature of BSP). The parameters used for estimating K for the 2 ft pipe were: D of 0.29 m (since the pipe could not cross a layer); an estimated Q of 0.1133 m^3/s and therefore a v of 1.715 m/s; and a pipe length of 104 m. This resulted in a K value of 18. If the pipe diameter of 0.6096 m (2 ft) had been used, the K would be 7.6. The parameters used for estimating K for the 3.5 in. pipe were: D of 0.09 m; an estimated Q of 0.028 m^3/s and therefore a v of 4.4 m/s; and a pipe length of 1.524 m. This resulted in a K value of 2.8.

It was not possible to get the exact parameters of the 2 ft diameter pipe. When talking to Laurie Dries, she stated that since this pipe has been modified over the history of BSP, it is difficult to determine exact parameters for the pipe. The pipe is 2 ft in diameter and the bathymetry at the location was measured to be 1.6 feet, meaning the

pipe is not fully submerged. However, the pipe then travels for approximately 104 m along the edge of BSP, dropping approximately 1.2 m along this length, before discharging into the bypass. Figure E.4 shows the pipe discharging into the bypass, along with a location of bypass leakage (the fountain of water behind the pipe outflow; the picture was taken prior to bypass repairs). From the figure, it appears that the pipe is flowing full when it discharges to the bypass. The problem then arises of determining where the pipe becomes full, and what the head shape looks like inside of the pipe. However, as was discussed above, pipes are required to be less than 0.3 m in diameter for the model, meaning that the 2 ft pipe was modeled as being fully submerged and therefore flowing full at its entrance, instead of partially full as it is in real life. The model is capable of modeling partially full pipes, but a coefficient C for the following equation must be specified.

$$Q = CA\sqrt{gh} \tag{E.6}$$

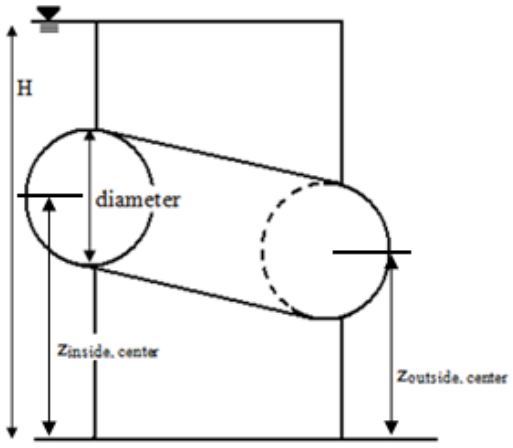

Figure E.3. Pipe setup for modeling.

Figure E.4. Discharge from the 2 foot pipe into the bypass. The apparent fountain behind the discharge is due to bypass leakage prior to repairs.

References

AHAB (2013). Chiroptera. from Airborne Hydrograph AB, http://www.airbornehydro.com/chiropter, accessed July 5, 2013.

Botelho, D., Imberger, J., Dallimore, C., and Hodges, B. R. (2009). A hydrostatic/non-hydrostatic grid-switching strategy for computing high-frequency, high wave number motions embedded in geophysical flows, *Environmental Modelling & Software, 24* (4), 473-488.

Brater, E. F., King, H. W., Lindell, J. E., and Wei, C. (1996). *Handbook of Hydraulics.* McGraw Hill.

Casulli, V., and Cheng, R. (1992). Semi-implicit finite-difference methods for 3-dimensional shallow-water flow. *International Journal for Numerical Methods in Fluids , 15* (6), 629-648.

Casulli, V., and Cattani, E. (1994). Stability, accuracy and efficiency of a semi-implicit method for 3-dimensional shallow-water flow. *Computers & Mathematics with Applications , 27* (4), 99-112.

Casulli, V. and Zanolli, P. (2002). Semi-Implicit Numerical Modeling of Nonhydrostatic Free-Surface Flows for Environmental Problems. *Mathematical and Computer Modelling, 36* (9-10), 1131-1149.

Cerco, C.F., Cole, T. (1993). 3-Dimensional Eutrophication Model of Chesapeake Bay. *Journal of Environmental Engineering – ASCE 119* (6), 1006-1025.

Chippindale, P. T., Price, A. H., and Hillis, D. M. (1993). A New Species of Perennibranchiatte Salamander (Eurycea: Plethodontidae) from Austin, Texas. *Herpetologica , 49* (2), 248-259.

City of Austin. (1998). Final environmental assessment/habitat conservation plan for issuance of a section 10(a)(B) permit for incidental take of the Barton Springs salamander (Eurycea sosorum) for the operation and maintenance of Barton Springs Pool and adjacent springs. Austin.

Colucci, L. (2009). Barton Springs Pool beach recirculation pilot project. City of Austin, Watershed Protection Department. Short Report SR-09-04.

Dallimore, C. J., Hodges, B. R., and Imberger, J. (2003), Coupling an Underflow Model to a Three-Dimensional Hydrodynamic Model. *Journal of Hydraulic Engineering-ASCE, 129* (10), 748-757.

FAA 2008, Global Positioning System Wide Area Augmentation System (WAAS) Performance Standard, 1st edition, Federal Aviation Administration, Washington DC, 60 pgs. URL: http://www.gps.gov/technical/ps/2008-WAAS-performance-standard.pdf , accessed 7/20/2013.

Fong, D., and Monismith, S. (2004). Evaluation of the accuracy of a ship-mounted, bottom-tracking ADCP in a near-shore coastal environment. *Journal of Atmospheric & Oceanic Technology , 21* (7), 1121-1128.

GPS.gov (2013) GPS Accuracy, URL: http://www.gps.gov/systems/gps/performance/accuracy/, accessed 7/20/2013.

Hodges, B.R. (2013). Hydrodynamical Modeling. In: Gene E. Likens, (Editor) *Encyclopedia of Inland Waters*. Oxford: Elsevier.

Hodges, B. R., Imberger, J., Saggio A., and Winters, K. B. (2000), Modeling Basin-Scale Internal Waves in a Stratified Lake. *Limnology and Oceanography, 45* (7), 1603-1620.

Hodges, B., Laval, B., and Wadzuk, B. (2006). Numerical error assessment and a temporal horizon for internal waves in a hydrostatic model. *Ocean Modeling , 13* (1), 44-64.

Hodges, B. R., and Rueda, F. J. (2008). Semi-implicit two-level predictor-corrector methods for non-linearly coupled, hydrostatic, barotropic/baroclinic flows. *International Journal of Computational Fluid Dynamics , 22* (9), 593-607.

Hunt, B. B., Banda, N., and Smith, B. A. (2010). Three-dimensional geologic model of the Barton Springs segment of the Edwards Aquifer, Central Texas. *Gulf Coast Association of Geological Societies Transactions 60*, 355-367.

Kantha, L., and Clayson, C. (2000). *Numerical Models of Oceans and Oceanic Processes.* Academic Press.

King, W., and Zheng, M. (2004). Department of Chemistry, Colby College.

Koçyigit, M. B., Falconer, R. A. (2004) Three-dimensional numerical modeling of wind-driven circulation in a homogenous lake. *Advances in Water Resources, 27* (12), 1167-1178.

Limbacher and Godfrey Architects (2008). Barton Springs Pool Master Plan, Concepts for Preservation and Improvement. Available at ftp://ftp.ci.austin.tx.us/, accessed 05/01/2013.

Lowrance (2011a). HDS-5 & HDS-7 Fish Finding Sonar and GPS Operations Guide. Tulsa, OK: Navico.

Lowrance (2011b). Sonar Log Viewer (Version 2.1.2) [Computer Program]. Available at http://www.lowrance.com/en-US/Support/Sonar-Log-Viewer/, accessed 03/02/2012.

Lowrance (2011c). HDS Series Installation Manual. Available at http://www.lowrance.com/en-US/Products/Fishfinder-Chartplotter/HDS5-en-us.aspx/, accessed 01/09/2012.

Mahler, B., Garner, B., Musgrove, M., Guilfoyle, A., and Rao, M. (2006). Recent (2003-2005) water quality of Barton Springs, Austin, Texas, with emphasis factors affecting variability. U.S. Geological Survey Scientific Investigations Report 2006-5299: 83 p.

Mahler, B., Musgrove, M., Sample, T., and Wong, C. (2011). Recent (2008-2010) water quality in the Barton Srings Segment of hte Edwards Aquifer and its contributing zone, central Texas, with emphasis factors affecting nutrients and bacteria. U.S. Geological Survey Scientific Investigations Report 2011-5139, 66 p.

Scanlon, B., Mace, R., Smith, B., Hovorak, S., Dutton, A., and Reedy, R. (2001). Groundwater availibility of the Barton Srpings aquifer, Texas - Numerical simulations through 2050. Texas Bureau of Economic Geology for the lower Colorado River Authority, Under Conract UTA 99-0, 36 p.

Slade, R. J., Dorsey, M., and Stewart, S. (1986). Hydrology and water quality of the Edwards aquifer associated with Barton Springs in the Austin area, Texas. U.S. Geological Survey Water-Resources Investigations Report 86-4036, 117 p.

SonTek (2010). ViewArgonaut (Version 3.72) [Computer Program]. Available at http://www.sontek.com/sw/viewargonaut.php/, accessed 05/10/2013.

SonTek (2011). RiverSurveyor Live (Version 3.01) [Computer Program]. Available at http://www.sontek.com/riversurveyor-s5-m9.php, accessed 07/17/2012.

SonTek (2012a). HydroSurvey User's Manual. San Diego, CA: Xylem.

SonTek (2012b). HydroSurveyor (Version 1.2) [Computer Program]. Available at http://www.sontek.com/software.php/, accessed 12/19/2012.

Swamee, P., and Jain, A. (1976). Explicit equations for pipe-flow problems. *Journal of the Hydraulics Division- ASCE, 102* (5), 657-664.

Toomey, Michael (2010). KML-Matlab-Shapefile conversion (http://www.mathworks.com/matlabcentral/fileexchange/25104-kml-matlab-shapefile-conversion/content/kml_shapefile.m), MATLAB Central File Exchange., retrieved June 07, 2012.

Tuchsherer, R., Schroeder, G., and King, J. (2011). Structural Condition Assessment, Barton Springs Pool – Upstream and Downstream Dams. Prepared by Datum Engineers, Inc.

U.S. Fish and Wildife Service. (1997). Endangered and threatened wildlife: final rule to list the Barton Springs Salamander as Endangered. Federal Register 62: 23377-23392.

Wadzuk, B., and Hodges, B. (2004). Hydrostatic and Non-Hydrostatic Internal Wave Models, CRWR Online Report 04-09. 77. University of Texas at Austin. From http://www.crwr.utexas.edu/online.shtml.

Wadzuk, B., and Hodges, B. (2009). Hydrostatic versus nonhydrostatic Euler-equation modeling of nonlinear internal waves. *Journal of Eng. Mech., 135* (10), 1069-1080.

Weilbeer, H., and Jankowski, J. A. (2000). A three-dimensional non-hydrostatic model for free surface flows – development, verification, and limitations. *Proc. Of 6th International Conference in Estuarine and Coastal Modeling*, pp. 162-177.

Wadzuk, B., and Hodges, B. (2009). Hydrostatic versus nonhydrostatic Euler-equation modeling of nonlinear internal waves. *Journal of Engineering Mechanics, 135* (10), 1069-1080.

Wang, P. F., Cheng, R. T, and Richter, K. (1998). Modeling tidal hydrodynamics of San Diego Bay, California. *Journal of American Water Resources Association, 34* (5), 1123-1140.

Westerink, J. J., Luettich, R. A., Feyen, J. C., Atkinson, J. H., Dawson, C., Roberts, H. J., Powell, M. D., Dunion, J. P., Kubatko, E. J., and Pourtaheri, H. (2008). A basin-to channel-scale unstructured grid hurrican storm surge model applied to Louisiana. *Monthly Weather Review 136* (3), 833-864.

Wu, F. C., Shen, H. W., and Chou, Y. J. (1999). Variation of roughness coefficients for unsubmerged and submerged vegitation. *Journal of Hydraulic Engineering-ASCE, 125* (9), 934-942.